

# FRONT TRACKING FOR A MODEL OF IMMISCIBLE GAS FLOW WITH LARGE DATA

HELGE HOLDEN, NILS HENRIK RISEBRO, AND HILDE SANDE

ABSTRACT. In this paper we study front tracking for a model of one dimensional, immiscible flow of several isentropic gases, each governed by a gamma-law. The model consists of the  $p$ -system with variable gamma representing the different gases. The main result is the convergence of a front tracking algorithm to a weak solution, thereby giving existence as well. This convergence holds for general initial data with a total variation satisfying a specific bound. The result is illustrated by numerical examples.

## 1. INTRODUCTION

We want to describe the one dimensional, immiscible flow for several isentropic gases. The different gases are initially separated, and the pressure is for all gases given by a  $\gamma$ -law, that is,  $p = \rho^\gamma$ , where  $\rho$  is the density and  $\gamma$  is the adiabatic gas constant for each gas. We assume  $\gamma(x, t) > 1$ . In Lagrangian coordinates  $\gamma$  only depends on  $x$  because the different gases cannot mix. Thus, the flow of these gases is described for  $x \in \mathbb{R}$  and  $t \in (0, \infty)$  by the system

$$(1.1) \quad \begin{aligned} v_t - u_x &= 0, \\ u_t + p(v, \gamma)_x &= 0, \\ \gamma_t &= 0, \end{aligned}$$

where  $v = 1/\rho$  is the specific volume,  $u$  is the velocity, and  $p(v, \gamma) = v^{-\gamma}$  is the pressure function. This  $3 \times 3$  system of hyperbolic conservation laws is strictly hyperbolic for  $v < \infty$ .

We consider the Cauchy problem for this system, that is, system (1.1) with general initial data

$$(1.2) \quad v(x, 0) = v_0(x), \quad u(x, 0) = u_0(x), \quad \gamma(x, 0) = \gamma_0(x), \quad x \in \mathbb{R}.$$

Glimm [12] proved global existence of a weak solution of the Cauchy problem with initial data of small total variation for strictly hyperbolic systems where each family is either genuinely nonlinear or linearly degenerate, thus including the present system. This solution is found as a limit of the Glimm scheme [12] or of the front tracking method [13, 4]. In [14] we extended the existence result to large initial data for (1.1) by using the Glimm scheme. In this paper we prove that a front tracking algorithm converges to a weak solution, thereby giving an alternative existence argument.

---

*Date:* March 26, 2010.

*2000 Mathematics Subject Classification.* Primary: 35L65, 76N15; Secondary: 35A05.

*Key words and phrases.*  $p$ -system, gamma law, mixture of gases.

This paper was written as part of the international research program on Nonlinear Partial Differential Equations at the Centre for Advanced Study at the Norwegian Academy of Science and Letters in Oslo during the academic year 2008–09. Supported in part by the Research Council of Norway through the project “Integro-PDEs: Numerical methods, Analysis, and Applications to Finance”.

System (1.1) is an extension of the  $p$ -system

$$(1.3) \quad \begin{aligned} v_t - u_x &= 0, \\ u_t + p(v)_x &= 0, \end{aligned}$$

which describes the flow of one isentropic gas. The parameter  $\gamma$  is constant, and the pressure, still given by a  $\gamma$ -law, is a function of  $v$  only. For the  $p$ -system with  $\gamma = 1$ , Nishida [18] showed existence of a global weak solution for arbitrary bounded initial data. For  $\gamma > 1$ , Nishida and Smoller [19] proved existence of a weak solution for initial data where  $(\gamma - 1)$  times the total variation of the initial data is sufficiently small. The case with large initial data for  $2 \times 2$  systems is also discussed in [5, 9].

The system (1.1) does not have a coordinate system of Riemann invariants, only a 2-Riemann coordinate. Therefore we do not have the advantage of changing variables to Riemann invariants as for the  $p$ -system and other  $2 \times 2$  systems. Liu [15] proved existence of a solution for the full Euler system with large initial data, another  $3 \times 3$  system without a coordinate system of Riemann invariants. Liu's change of variables is inspired by the use of Riemann invariants, but a similar approach does not simplify system (1.1) because  $\gamma$  is a function of  $x$ . The general results by Temple [23] include both the results of [19] and [15]. In [23] one considers the flux function as a smooth one-parameter family of functions where one has existence of a solution for initial data in  $B.V.$  when this parameter  $\epsilon$  is equal to zero. Then the system with  $0 \leq \epsilon \leq 1$  has a unique solution if  $\epsilon$  times the total variation of the initial data is sufficiently small. Letting  $\epsilon = \gamma - 1$  for the  $p$ -system and the Euler equations, one obtains similar results as in [19] and [15]. However, this approach cannot be used for system (1.1) since  $\gamma$  is one of the variables. Wissman proved in [27] a large data existence theorem for the  $3 \times 3$  system of relativistic Euler equations in the ultra-relativistic limit. Applying a change of coordinates the shock waves become translation invariant and a Nishida-type of analysis is used.

For  $3 \times 3$  systems with a 2-Riemann coordinate, Temple and Young [24] showed existence of a solution for initial data with arbitrary large total variation, provided that the oscillations are small. This result applies to (1.1) as well, but we want to avoid the restriction on the oscillations. Peng [21, 20] also considered certain  $3 \times 3$  systems (Lagrangian gas dynamics for a perfect gas and a model originating in multiphase flow modeling) with large initial data.

All these existence results are proved using the Glimm scheme. Asakura shows the convergence of front tracking for the  $p$ -system [3] and for the Euler equations [2] with large initial data. The conditions on the initial data are the same as obtained in [19] and [15]. In [7, 8] front tracking is used to study systems of conservation laws whose flux functions depend on a parameter vector,  $\mu$ , similar to those in [23]. An approach for establishing  $L^1$ -estimate point-wise in time between entropy solutions for  $\mu \neq 0$  and  $\mu = 0$  is given. In particular, letting  $\mu = \gamma - 1$ , the  $L^1$ -estimate between entropy solutions in the large for the isentropic Euler equations and the isothermal Euler equations is established in [7] and between entropy solutions in the large for the Euler equations and the isothermal Euler equations in [8].

Amadori and Corli [1] extend the  $p$ -system with an extra equation,  $\lambda_t = 0$ , to model multiphase flow, and use front tracking to prove existence of a weak solution for large data. As for system (1.1), the pressure function in [1] is a function of both  $v$  and the new variable,  $\lambda$ , making the two systems similar. However, since the adiabatic gas constant,  $\gamma$ , is equal to one in [1], vacuum can never occur for their system as it can for system (1.1). Furthermore, the wave curves in [1] are monotone in  $\lambda$ , resulting in a considerably simpler analysis of the wave interactions compared with the analysis necessary for the model considered here. The system treated in [1] is a simplified version of the model discussed by Fan in [11]. Similar

models, but with a rather different pressure law, are also considered in [10] and [17] applying completely different methods. A model in the context of the Navier–Stokes equation with finitely many independent pressure laws has been studied in [6].

System (1.1) can also be rewritten as a  $2 \times 2$  system with discontinuous flux. We get

$$\begin{aligned} v_t - u_x &= 0, \\ u_t + p(v, \gamma(x))_x &= 0, \end{aligned}$$

where the adiabatic gas constant of the different gases is given by the discontinuous function  $\gamma(x)$ .

The rest of the paper is organized as follows: In Section 2 we discuss the wave curves of the system. The variable  $\gamma$  is constant along the rarefaction and shock waves of the first and third family, therefore these curves are similar to the wave curves of the  $p$ -system. However, these curves are not monotone in  $\gamma$ , which considerably complicates the interactions of waves with different values of  $\gamma$ . The second family is linearly degenerate and gives rise to a contact discontinuity along which  $p$  and  $u$  are constant. Thus, by changing variables to  $p$ ,  $u$  and  $\gamma$ , the Riemann problem is easy to describe.

Section 3 is the main part of this paper where we first present the front-tracking algorithm. The solution of any Riemann problem is made piecewise constant by approximating rarefaction waves as step functions. In addition, a simplified Riemann solver generating non-physical fronts is introduced in order to ensure that the number of fronts remains finite. The simplified solver is only used for interactions where a 1- or 3 front collides with a contact discontinuity and the product of their strengths is less than some threshold parameter. This solver generates non-physical fronts, traveling either to the left or the right, with absolute speed larger than any other front. Moreover, when a non-physical front collides with another front, it just passes through without changing the strength or type of the front. Multiple interactions, that is, interactions between more than two fronts, are avoided in the algorithm by shifting the speed of some of the fronts by a small amount so that no more than two fronts interact at a given point. In Section 3.2 we define a Glimm functional and show that it is decreasing under the conditions given in Proposition 3.5 by considering all possible interactions. We use this to show that there is a finite number of interactions up to any given time, hence, the front-tracking algorithm is well-defined. Furthermore, we bound the total amount of non-physical fronts present at any time in a similar manner as in [1] by introducing a generation concept. Note that the interaction estimates are only valid away from vacuum, see [16], however, whenever the conditions on the initial data given in Lemma 3.13 and by (3.35) are satisfied, the approximate solution found using front tracking has bounded total variation and is bounded away from vacuum. We end Section 3 by proving that the sequence of approximate solutions converges to a weak solution of the system. This proves the main theorem:

**Theorem 3.14.** *Assume that  $(\sup(\gamma(\cdot, 0)) - 1)\text{T.V.}(p(\cdot, 0), u(\cdot, 0))$  and  $\text{T.V.}(\gamma(\cdot, 0))$  are sufficiently small. Then the front tracking algorithm is well-defined and gives a sequence which converges to a weak solution of (1.1).*

Observe that by reducing the total variation of  $\gamma$  and reducing its supremum, one can allow for arbitrary large total variation of  $p$  and  $u$ . Due to Wagner [25], this result translates into existence for the system (3.45) in Eulerian coordinates.

In the last section we study some examples numerically. In the first example we have one gas confined to an interval, surrounded by another gas. The two gases have distinct but constant gammas. The constants that limit the total variation of the initial data are computed, and the initial data are chosen so that they satisfy

the conditions in the theorem. The Glimm functional is explicitly computed, and we observe decay in accordance with the theorem. In the second example the initial data are piecewise constant, while  $\gamma$  is continuously varying in the third example. For these two examples, the total variation of the chosen initial data do not satisfy the theorem, nevertheless we still observe that the Glimm functional is decaying.

## 2. THE SYSTEM

It is well-known that systems of hyperbolic conservation laws such as (1.1) do not in general have smooth solutions, even for smooth initial data. Thus, by a solution of (1.1) with the initial data (1.2) we mean a *weak solution* in the distributional sense with  $(v, u, \gamma) \in L^1_{\text{loc}}(\mathbb{R} \times [0, \infty))$  so that

$$(2.1) \quad \begin{aligned} \iint_{\mathbb{R} \times [0, \infty)} (v\phi_t - u\phi_x) dxdt + \int_{\mathbb{R}} v_0(x)\phi(x, 0) dx &= 0, \\ \iint_{\mathbb{R} \times [0, \infty)} (u\phi_t + p\phi_x) dxdt + \int_{\mathbb{R}} u_0(x)\phi(x, 0) dx &= 0, \\ \iint_{\mathbb{R} \times [0, \infty)} \gamma\phi_t dxdt + \int_{\mathbb{R}} \gamma_0(x)\phi(x, 0) dx &= 0, \end{aligned}$$

for all test function  $\phi \in C_0^\infty(\mathbb{R} \times [0, \infty))$ . Note that the functions

$$\eta(v, u, \gamma) = \frac{1}{2}u^2 - \int^v p(\tau, \gamma) d\tau + h(\gamma), \quad q(v, u, \gamma) = up(v, \gamma),$$

form an entropy/entropy flux pair for system (1.1) for some function  $h(\gamma)$ .

If the specific volume,  $v$ , becomes infinite, which corresponds to zero density and zero pressure, we have *vacuum*. At vacuum, the properties of the system change and the methods used here do not apply, therefore we only consider system (1.1) for  $v(x, t) < \infty$ . Furthermore, we assume  $\gamma(x, t) > 1$ .

We write  $U(x, t) = (v(x, t), u(x, t), \gamma(x, t))$ . Often we will work with  $p$  instead of  $v$ , and then also write  $U(x, t) = (p(x, t), u(x, t), \gamma(x, t))$ .

For  $v < \infty$ , or equivalently,  $p > 0$ , system (1.1) is strictly hyperbolic with eigenvalues

$$(2.2) \quad \lambda_1 = -\lambda, \quad \lambda_2 = 0, \quad \lambda_3 = \lambda,$$

where  $\lambda := \sqrt{-p_v} = \sqrt{\gamma v^{-\gamma-1}}$ , and corresponding eigenvectors

$$(2.3) \quad r_1 = (1, \lambda, 0), \quad r_2 = (-p_\gamma, 0, p_v), \quad r_3 = (-1, \lambda, 0).$$

Note that the eigenvalues and eigenvectors do not depend on  $u$ . The first and the third family are genuinely nonlinear, while the second family is linearly degenerate. Moreover, the system does not possess a coordinate system of Riemann invariants, but  $\gamma$  is a Riemann coordinate for the second family.

Before we turn to solving system (1.1) with general initial data, we need to solve the Riemann problem for (1.1), that is, when the initial data consists of two constant states separated by a jump,

$$(2.4) \quad U(x, 0) = \begin{cases} U_l, & \text{if } x < 0, \\ U_r, & \text{if } x > 0. \end{cases}$$

The solution of the Riemann problem consists of up to three elementary *waves*, one from each family, and up to two intermediate constant states separating these waves. Thus, we start by looking at the wave curves.

For the genuinely nonlinear families there are two types of waves: We have *rarefaction waves* which are continuous waves of the form  $U(x, t) = w(x/t) = w(\xi)$

satisfying

$$(2.5) \quad \dot{w}(\xi) = r_j(w(\xi)), \quad \lambda_j(w(\xi)) = \xi, \quad j = 1, 3,$$

where  $\lambda_j$  is increasing along the wave, thus, the rarefaction solution is of the form

$$(2.6) \quad U(x, t) = \begin{cases} U_l, & \text{if } x < \lambda_j(U_l)t, \\ w(x/t), & \text{if } \lambda_j(U_l)t < x < \lambda_j(U_r)t, \\ U_r, & \text{if } x > \lambda_j(U_r)t. \end{cases}$$

Furthermore, we have *shock waves* which are solutions

$$(2.7) \quad U(x, t) = \begin{cases} U_l, & \text{if } x < \sigma_j t, \\ U_r, & \text{if } x > \sigma_j t, \end{cases}$$

satisfying the Rankine–Hugoniot condition

$$(2.8) \quad \sigma_j(U_r - U_l) = f(U_r) - f(U_l), \quad j = 1, 3,$$

for a shock velocity  $\sigma_j$ . The admissible shock waves are those satisfying the Lax entropy conditions

$$(2.9) \quad \lambda_{j-1}(U_l) < \sigma_j < \lambda_j(U_l), \quad \lambda_j(U_r) < \sigma_j < \lambda_{j+1}(U_r), \quad j = 1, 3.$$

For the linearly degenerate family  $j = 2$  there is only one type of waves called *contact discontinuities*. These waves are solutions of the form (2.7) which satisfy the Rankine–Hugoniot condition (2.8) with  $\sigma = \lambda_2 = 0$ . For system (1.1) we observe that  $\gamma$  changes only along these contact discontinuities. Moreover, both  $u$  and  $p = v^{-\gamma}$  are constant along a contact discontinuity, and we therefore choose to work with the variables  $p$ ,  $u$  and  $\gamma$  from here on.

Fix a left state  $U_l = (p_l, u_l, \gamma_l)$ . For each family the *wave curve* consists of all states  $U$  that can be connected to the given left state by a wave of this family. A shock or a rarefaction curve through  $U_l$  lies in the plane  $\gamma = \gamma_l$  and is equal to the corresponding wave curve for the  $p$ -system (1.3) with  $\gamma = \gamma_l$ . The wave curves of system (1.1), as depicted in Figure 1, are given by

$$(2.10) \quad \Phi_1(p, U_l) := \begin{cases} (p, u_l - r(p, p_l, \gamma_l), \gamma_l), & p < p_l, \\ (p, u_l - s(p, p_l, \gamma_l), \gamma_l), & p > p_l, \end{cases}$$

$$(2.11) \quad \Phi_2(\gamma, U_l) := (p_l, u_l, \gamma), \quad \gamma > 1,$$

$$(2.12) \quad \Phi_3(p, U_l) := \begin{cases} (p, u_l + r(p, p_l, \gamma_l), \gamma_l), & p > p_l, \\ (p, u_l - s(p, p_l, \gamma_l), \gamma_l), & p < p_l, \end{cases}$$

where

$$(2.13) \quad r(p, p_l, \gamma_l) := \frac{2\sqrt{\gamma_l}}{\gamma_l - 1} \left( p^{\frac{\gamma_l-1}{2\gamma_l}} - p_l^{\frac{\gamma_l-1}{2\gamma_l}} \right),$$

$$(2.14) \quad s(p, p_l, \gamma_l) := \left( \left( p_l^{-\frac{1}{\gamma_l}} - p^{-\frac{1}{\gamma_l}} \right) (p - p_l) \right)^{1/2}.$$

Moreover, the shock velocities do not depend on  $u$  and are given by

$$(2.15) \quad \begin{aligned} \sigma_1(U_l, U) &= -\sigma(p_l, p), \\ \sigma_3(U_l, U) &= \sigma(p_l, p), \end{aligned} \quad \text{where } \sigma(p_l, p) = \sqrt{\frac{p - p_l}{p_l^{-1/\gamma_l} - p^{-1/\gamma_l}}}.$$

Finally, we mention the *backward 3-wave curve*, that is, the curve of all left states  $U$  that can be connected to a given right state  $U_r$  by a 3-wave;

$$(2.16) \quad \tilde{\Phi}_3(p, U_r) := \begin{cases} (p, u_r - r(p_r, p, \gamma_r), \gamma_r), & p < p_r, \\ (p, u_r + s(p_r, p, \gamma_r), \gamma_r), & p > p_r. \end{cases}$$

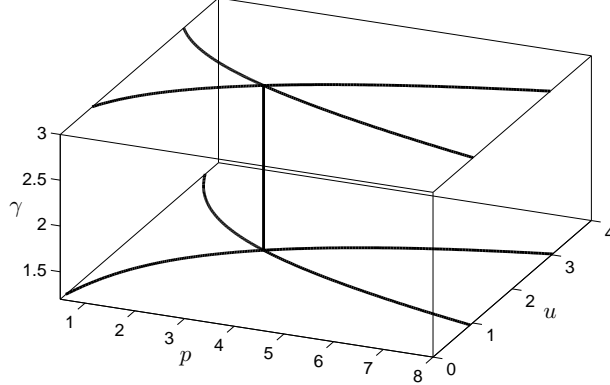


FIGURE 1. The wave curves through two left states with different  $\gamma$ .

Recall that if  $p = 0$ , we have vacuum, therefore, the wave curves are only well-defined for  $p > 0$  and  $p_l > 0$ . All results are for waves contained in

$$(2.17) \quad \mathcal{D} = \{(p, u, \gamma) \mid p \in [p_{\min}, p_{\max}], |u| < \infty, \gamma \in (1, \bar{\gamma}]\},$$

where  $p_{\min} > 0$ ,  $p_{\max} < \infty$  and  $\bar{\gamma} \in (1, \infty)$  are constants. For initial data given by (1.2) the upper and lower bound on  $p$  will be determined by (3.35) and we will show that

$$(2.18) \quad \bar{\gamma} := \sup_x (\gamma_0(x)),$$

for all waves. We moreover have an upper bound on the wave speed for all waves (or fronts) contained in  $\mathcal{D}$ , and we define

$$(2.19) \quad \lambda_{\max} = \max_{U \in \mathcal{D}} \{|\lambda_j|, |\sigma_j|\} = \max_{U \in \mathcal{D}} \{|\lambda_j|\},$$

where the last equality is due to the Lax entropy condition (2.9).

**Lemma 2.1.** *The wave curves in  $\mathcal{D}$  have the following properties:*

- (i) *The function  $\Phi_1$  is strictly decreasing and the function  $\Phi_3$  is strictly increasing when considered as functions of  $p$ .*
- (ii) *Given two wave curves,  $\Phi_j(p, U_1)$  and  $\Phi_j(p, U_2)$  where  $j \in \{1, 3\}$ , so that  $U_1$  is not on  $\Phi_j(p, U_2)$  and  $U_2$  is not on  $\Phi_j(p, U_1)$ . Then the two wave curves never intersect.*
- (iii) *Consider the projections onto the  $(p, u)$ -plane of the wave curves through  $U_1 = (p_l, u_l, \gamma_1)$  and  $U_1 = (p_l, u_l, \gamma_2)$  where  $\gamma_1 \leq \gamma_2$ . If*

$$\frac{\partial}{\partial p} r(p_l, p_l, \gamma_1) < \frac{\partial}{\partial p} r(p_l, p_l, \gamma_2),$$

*then the projected wave curves going to the right (with respect to  $p$ ) will never intersect, while the projected wave curves going to the left will intersect as  $p$  decreases. If*

$$\frac{\partial}{\partial p} r(p_l, p_l, \gamma_1) > \frac{\partial}{\partial p} r(p_l, p_l, \gamma_2),$$

*then the projected wave curves going to the right will intersect, while the projected wave curves going to the left will not. If*

$$\frac{\partial}{\partial p} r(p_l, p_l, \gamma_1) = \frac{\partial}{\partial p} r(p_l, p_l, \gamma_2),$$

*then none of the projected wave curves will intersect.*

- (iv) The slope of a rarefaction wave in the plane  $\gamma = \gamma_l$ ,  $\partial r / \partial p$ , only depends on  $p$  and  $\gamma_l$ , not on  $p_l$ . Furthermore, there exist two constants  $r'_{\min}$  and  $r'_{\max}$  only depending on  $p_{\min}$ ,  $p_{\max}$  and  $\bar{\gamma}$  so that

$$r'_{\min} \leq \frac{\partial}{\partial p} r(p, p_l, \gamma_l) \leq r'_{\max}.$$

- (v) The slope of a shock wave in the plane  $\gamma = \gamma_l$ ,  $\partial s / \partial p$ , depends on  $p$ ,  $\gamma_l$  and  $p_l$ . Furthermore, there exist two constants  $s'_{\min}$  and  $s'_{\max}$  only depending on  $p_{\min}$ ,  $p_{\max}$  and  $\bar{\gamma}$  so that

$$s'_{\min} \leq \frac{\partial}{\partial p} s(p, p_l, \gamma_l) \leq s'_{\max}.$$

- (vi) The wave curves have a continuous derivative at  $U_l$ ,

$$\lim_{p \rightarrow p_l} \frac{\partial}{\partial p} s(p, p_l, \gamma_l) = \frac{\partial}{\partial p} r(p_l, p_l, \gamma_l).$$

Furthermore,

$$\frac{\partial}{\partial p} s(p, p_l, \gamma_l) \geq \frac{\partial}{\partial p} r(p, p_l, \gamma_l),$$

for all  $p_l$ . Hence, a shock wave is always steeper than a rarefaction wave at a given  $p \neq p_l$ , provided both waves lie in the plane  $\gamma = \gamma_l$ .

- (vii) Rarefaction waves are additive; if a rarefaction wave connects  $U_1$  to  $U_2$  and another rarefaction wave of the same family connects  $U_2$  to  $U_3$ , then the rarefaction wave connecting  $U_1$  to  $U_3$  equals the concatenation of the other two rarefaction waves.
- (viii) Given two 1-shock waves starting at  $(p_1, u, \gamma)$  and  $(p_2, u, \gamma)$ , respectively, and assume  $p_1 < p_2$ . Then the shock wave starting at  $p_1$  is steeper than the shock wave starting at  $p_2$  at any given point  $p$ , that is,

$$\frac{\partial}{\partial p} s(p, p_2, \gamma) < \frac{\partial}{\partial p} s(p, p_1, \gamma),$$

for all  $p \geq p_2 > p_1$ .

- (ix) Given two 3-shock waves starting at  $(p_1, u, \gamma)$  and  $(p_2, u, \gamma)$ , respectively, and assume  $p_1 < p_2$ . Then the shock wave starting at  $p_2$  is steeper than the shock wave starting at  $p_1$  at any given point  $p$ , that is,

$$\frac{\partial}{\partial p} s(p, p_1, \gamma) < \frac{\partial}{\partial p} s(p, p_2, \gamma),$$

for all  $p \leq p_1 < p_2$ .

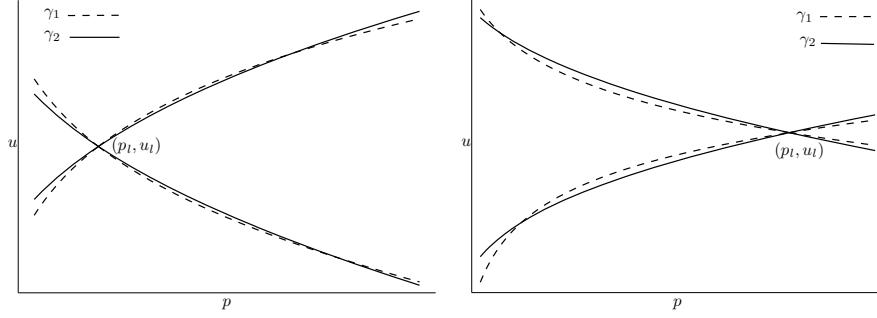
*Proof.* All the properties follows from differentiating the wave curves.  $\square$

The projection onto the  $(p, u)$ -plane of two wave curves with different  $\gamma$ 's are shown in Figure 2. Note that the projected wave curves intersect, cf. property (iii), because the slopes of the projected wave curves depend on  $\gamma$ . The next lemma gives an estimate on how different two waves with different  $\gamma$ 's are.

**Lemma 2.2.** *Let  $\epsilon_1$  and  $\epsilon_2$  be 1-waves of the same type such that  $\epsilon_1$  connects  $(p_0, u_0, \gamma_1)$  to  $(p, u_1, \gamma_1)$  and  $\epsilon_2$  connects  $(p_0, u_0, \gamma_2)$  to  $(p, u_2, \gamma_2)$ , or let  $\eta_1$  and  $\eta_2$  be 3-waves of the same type such that  $\eta_1$  connects  $(p, u_1, \gamma_1)$  to  $(p_0, u_0, \gamma_1)$  and  $\eta_2$  connects  $(p, u_2, \gamma_2)$  to  $(p_0, u_0, \gamma_2)$ . Assume that all waves are contained in  $\mathcal{D}$  and that  $u_1 < u_2$ . Then*

$$(2.20) \quad u_2 - u_1 \leq c_2 |p - p_0| |\gamma_2 - \gamma_1|,$$

where  $c_2$  only depends on  $p_{\min}$ ,  $p_{\max}$  and  $\bar{\gamma}$ .



(a) Here  $\frac{\partial}{\partial p} r(p_l, p_l, \gamma_1) > \frac{\partial}{\partial p} r(p_l, p_l, \gamma_2)$ , thus, the projected wave curves going to the right intersect. (b) Here  $\frac{\partial}{\partial p} r(p_l, p_l, \gamma_1) < \frac{\partial}{\partial p} r(p_l, p_l, \gamma_2)$ , thus, the projected wave curves going to the left intersect.

FIGURE 2. The wave curves through  $U_1 = (p_l, u_l, \gamma_1)$  (dotted line) and  $U_2 = (p_l, u_l, \gamma_2)$ , where  $\gamma_1 < \gamma_2$ , projected onto the  $(p, u)$ -plane.

Note that for 1-waves we compare two waves where the projected waves start at the same point in the  $(p, u)$ -plane, while we for 3-waves compare two waves where the projected waves end at the same point. The proof of this lemma is given in [14] and is based on the techniques used in [26].

We are now ready to discuss the Riemann Problem, that is, solving (1.1) with initial data given by (2.4).

**Lemma 2.3.** *The Riemann problem for (1.1) where  $U_l$  and  $U_r$  are contained in  $\mathcal{D}$ , cf. (2.17), has a unique solution without vacuum if*

$$(2.21) \quad u_r - u_l < r(p_r, 0, \gamma_r) - r(0, p_l, \gamma_l).$$

*Proof.* Note that if  $\gamma_l = \gamma_r$ , then the Riemann problem for (1.1) reduces to the Riemann problem for the  $p$ -system (1.3). The solution of this problem is described in detail in [22, Ch. 17, §A], and it is unique if (2.21) is satisfied with  $\gamma_l = \gamma_r$ .

A 2-wave takes us from one plane,  $\gamma = \gamma_1$ , to another plane,  $\gamma = \gamma_2$ , while  $p$  and  $u$  remain constant. Therefore, the Riemann problem has a unique solution if the projections onto the  $(p, u)$ -plane of the 1-wave curve,  $\Phi_1(p, U_l)$ , and the backward 3-wave curve,  $\tilde{\Phi}_3(p, U_r)$ , have a unique intersection point. From property (i) of Lemma 2.1 we have that the projection of  $\Phi_1$  is strictly decreasing in  $p$  and it follows that the projection of  $\tilde{\Phi}_3$  is strictly increasing in  $p$ . Hence, the projected curves intersect at most once. The only way the two curves do not intersect is if the projection of the backward 3-rarefaction wave from  $U_r$  always lies above the projection of the 1-rarefaction wave from  $U_l$ . Thus, if

$$u_r - r(p_r, 0, \gamma_r) < u_l - r(0, p_l, \gamma_l),$$

then the projections of  $\tilde{\Phi}_3(p, U_r)$  and  $\Phi_1(p, U_l)$  onto the  $(p, u)$ -plane have a unique intersection point, and the Riemann problem has a unique solution.  $\square$

The solution of the Riemann problem  $(U_l, U_r)$  is constructed as follows: Let  $(\tilde{p}, \tilde{u})$  be the unique intersection between the projections of  $\Phi_1(p, U_l)$  and  $\tilde{\Phi}_3(p, U_r)$  onto the  $(p, u)$ -plane. We connect  $U_l = (p_l, u_l, \gamma_l)$  to  $\tilde{U}_1 = (\tilde{p}, \tilde{u}, \gamma_l)$  by a 1-wave, then we go from  $\tilde{U}_1$  to  $\tilde{U}_2 = (\tilde{p}, \tilde{u}, \gamma_r)$  along a contact discontinuity, and finally connect  $\tilde{U}_2$  to  $U_r = (p_r, u_r, \gamma_r)$  by a 3-wave.

Note that due to the varying  $\gamma$  there is no invariant region for the Riemann problem for system (1.1).

## 3. THE CAUCHY PROBLEM

We now turn to the Cauchy problem and use front tracking to obtain a sequence of approximate solutions. The goal of this section is to show that a subsequence converges to a weak solution of (1.1). In order to do this, we find a suitable Glimm functional and show that it decreases in time. First we need some notation, let

$$\begin{array}{lll} \epsilon \text{ define a 1-wave,} & \alpha \text{ a 1-shock wave,} & \mu \text{ a 1-rarefaction wave,} \\ \eta \text{ a 3-wave,} & \beta \text{ a 3-shock wave,} & \nu \text{ a 3-rarefaction wave,} \\ \zeta \text{ a 2-wave,} & \theta \text{ a 1- or 3-wave,} & \end{array}$$

Furthermore, we define *the strength of a 1-wave* or *a 3-wave* as the jump in  $p$  across the wave and *the strength of a 2-wave* as the jump in  $\gamma$  across the wave. The strength of a wave (or a front) is denoted by  $|\theta|$ . We are now ready to discuss front tracking and to define fronts. Note that we will use the above notation for fronts as well as waves. In addition, we will define non-physical fronts which will be denoted by  $\theta^{\text{np}}$  and *the strength of a non-physical front* will be defined as its jump in  $u$ . Since there is no invariant region for system (1.1), we start by considering initial data bounded away from vacuum in a neighborhood to a reference state. Later we give conditions on the initial data so that the solution found using front tracking always stays in a domain on the form (2.17).

**3.1. Front tracking.** The key point of front tracking is the approximation of the Riemann solutions, as will be described in detail below, yielding a piecewise constant solution. The discontinuities in the solution are called *fronts* and move with finite speeds. When two fronts collide at a *collision point*  $(x, \tau)$ , we say that they *interact* and refer to the colliding fronts as *incoming fronts*. If more than two fronts collide we have a *multiple collision* which will be resolved into a sequence of interactions between two fronts. Furthermore, the fronts resulting from solving the Riemann problem defined by the states immediately to the left and right of the incoming fronts are called *outgoing fronts* and are usually denoted with a prime. With this notation at hand, the front-tracking method used in this paper can be described as follows: Define three parameters  $\delta, \delta_{\text{init}}, \delta_\sigma > 0$ , so that  $\delta_{\text{init}}$  and  $\delta_\sigma$  tend to zero as  $\delta$  tends to zero, and fix a threshold parameter  $\rho > 0$ . First, approximate the initial data  $U_0$  by a piecewise constant function  $U_0^{\delta_{\text{init}}}$ , so that

$$\lim_{\delta_{\text{init}} \rightarrow 0} \|U_0^{\delta_{\text{init}}} - U_0\|_{L^1} = 0.$$

where  $\delta_{\text{init}}$  is the distance between the discontinuities. Then solve the Riemann problems defined by the jumps in  $U_0^{\delta_{\text{init}}}$  using the approximate Riemann solver. Track all fronts until the first interaction. If this is a multiple collision, change the speed of some of the fronts by  $\delta_\sigma$ , see Lemma 3.2, and track again. The Riemann problem at the interaction point is solved using the approximate Riemann solver unless it is an interaction between a contact discontinuity  $\zeta$  and another front  $\theta$  for which

$$(3.1) \quad |\theta| |\zeta| \leq \rho,$$

then the simplified Riemann solver is used. Keep tracking the fronts and solving the Riemann problems until there are no more interactions or a given time is reached.

Note that for system (1.1), we can ensure that no vacuum forms at  $t = 0+$  by requiring that  $U_0^{\delta_{\text{init}}}$  satisfies (2.21) at every discontinuity.

The *approximate Riemann solver* solves all shocks and contact discontinuities exactly, but approximates the continuous rarefaction waves by a step function connecting the left state  $U_l$  to the right state  $U_r$ . Let  $k := \lceil |p_r - p_l| / \delta \rceil$ . The rarefaction wave is divided into  $k$  fronts, each with strength  $\hat{\delta} = |\theta| / k \leq \delta$ . For

a 1-rarefaction wave, these discontinuities move with the speed of the left state, while for a 3-rarefaction wave they move with the speed of the right state. By this slightly non-standard definition, the symmetry property of system (1.1), which will be discussed in Lemma 3.1, still holds. Note that the jumps in the approximated rarefaction wave do not satisfy the Rankine–Hugoniot condition, however, as shown in Section 3.6, the approximate solution converges to the exact weak solution as  $\delta$  tends to zero.

We call an interaction involving a contact discontinuity a  $\gamma$ -collision. If we have a  $\gamma$ -collision where the strengths of the incoming fronts satisfy (3.1), then the *simplified Riemann solver* is used. We get

$$\zeta + \epsilon \rightarrow \epsilon' + \zeta + \theta^{\text{np}}, \quad \text{or} \quad \eta + \zeta \rightarrow \theta^{\text{np}} + \zeta + \eta',$$

as illustrated in Figure 3(a) and 3(b), with intermediate states  $\tilde{U}_1 = (p_r, \tilde{u}, \gamma_l)$  and  $\tilde{U}_2 = (p_r, \tilde{u}, \gamma_r)$ , or  $\tilde{U}_1 = (p_l, \tilde{u}, \gamma_l)$  and  $\tilde{U}_2 = (p_l, \tilde{u}, \gamma_r)$ , respectively. The projection onto the  $(p, u)$ -plane of the interaction  $\zeta + \epsilon$  is depicted in Figure 10. Using the simplified solver only the contact discontinuity is solved exactly. Furthermore, we get one outgoing front of the same family and strength as the incoming one and a non-physical front across which only  $u$  varies. The non-physical front travels in the opposite direction of the incoming front with absolute speed  $\lambda_{\text{np}} > \lambda_{\text{max}}$ ; in this way the symmetry property, cf. Lemma 3.1, is retained for the simplified solver as well. In other words, our simplified solver introduces non-physical fronts with negative as well as positive speeds, and therefore differs slightly from the simplified solver introduced by Bressan [4]. We denote the non-physical fronts by  $\theta^{\text{np}}$  and recall that their strengths are defined by the jump in  $u$ . Whenever a non-physical

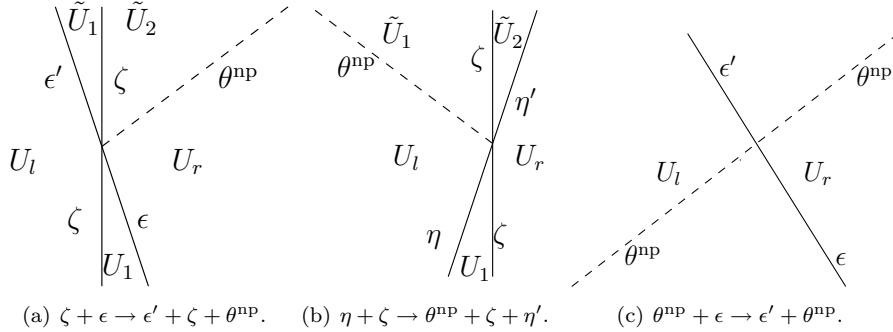


FIGURE 3. Interactions involving non-physical fronts (dashed lines).

front interacts with another front, as depicted in Figure 3(c), it just passes through the front. That is, both fronts have the same strengths as before, and are just shifted slightly in the  $u$ -direction. Note that all wave curves are invariant in the  $(p, u)$ -plane under a translation in  $u$ .

As discussed above, the approximate and simplified Riemann solvers are constructed so that the symmetry property of system (1.1) proved in [14] still holds. Formulated for fronts, this reads as follows:

**Lemma 3.1.** [14, Lemma 3.1] *Under the transformation  $x \mapsto -x$ , a 1-front connecting  $U_l$  to  $U_r$  becomes a 3-front connecting  $U_r$  to  $U_l$ , and vice versa. A 2-front is unchanged under this transformation, and a non-physical front becomes a non-physical front traveling in the opposite direction. Furthermore, the leftmost front with respect to  $x$  will become the rightmost front with respect to  $-x$ , and so on.*

Next, we discuss how we are able to remove any multiple collision by shifting the speed of some of the fronts.

**Lemma 3.2.** *Given a multiple collision between  $m$  fronts at  $(\hat{x}, \hat{\tau})$ . By shifting the speed of at most  $m - 2$  fronts by  $\delta_\sigma$  the multiple collision resolves, that is, the  $m$  fronts are only involved in interactions between two fronts. Moreover, no front present at any time  $t$  gets its speed shifted more than once.*

*Proof.* Let  $\hat{\tau}$  be the first time a multiple collision occurs, thus, none of the fronts present have got their speed shifted yet. We prove the lemma by induction on the number of fronts in the multiple interaction.

Assume first that three fronts interact at  $(\hat{x}, \hat{\tau})$ . Let  $\sigma_1$  be the speed of the leftmost front that is not a contact discontinuity and change this speed to  $\sigma_1 + \delta_\sigma$ . Then, this front will interact with the front to its right at a point  $(x_1, \tau_1)$  where  $\tau_1 < \hat{\tau}$ . One of the outgoing fronts of this interaction might interact with the third front for some time  $\tau_2 \leq \hat{\tau}$ , but this will also be an interaction between two fronts. Hence, by shifting the speed of one front, we are guaranteed that there is no multiple collision for  $t \leq \hat{\tau}$ . Moreover, the front with shifted speed will interact with another front at  $\tau_1 < \hat{\tau}$ , and can therefore never be part of any other multiple collision, in particular, can never get its speed shifted again.

Next, assume that we can resolve any multiple collision between  $i < n$  fronts by shifting the speed of at most  $i - 2$  fronts. Consider the case where  $n$  fronts interact at  $(\hat{x}, \hat{\tau})$ . We shift the speed of the leftmost front that is not a contact discontinuity by  $\delta_\sigma$ . Again, we get an interaction between this front and the front to its right at a point  $(x_1, \tau_1)$  where  $\tau_1 < \hat{\tau}$ . There are now three possible cases: (i) none of the outgoing fronts interact with any of the reminding  $n - 2$  fronts for any  $t \leq \hat{\tau}$ ; (ii) one of the outgoing fronts collides with the reminding  $n - 2$  fronts at  $(\hat{x}, \hat{\tau})$ ; (iii) one of the outgoing fronts interacts with the rightmost of the reminding  $n - 2$  fronts for some  $\tau_2 < \hat{\tau}$ . For cases (i) and (ii) we now have a multiple collision between  $n - 2$  and  $n - 1$  fronts, respectively, at  $(\hat{x}, \hat{\tau})$ , which we know how to resolve by shifting the speed of at most  $n - 4$  and  $n - 3$  fronts, respectively. In case (iii) we again have an interaction between two fronts at some  $\tau_2 < \hat{\tau}$ , resulting in the same three cases for the outgoing fronts, but now with  $n - 3$  reminding fronts colliding at  $(\hat{x}, \hat{\tau})$ . Continuing in this way, we conclude that a multiple collision between  $n$  fronts can be resolved by shifting the speed of at most  $n - 2$  fronts. Note also that the fronts with shifted speeds are all involved in an interaction with another front at some  $\tau \leq \hat{\tau}$ , and can therefore never be involved in further multiple collisions.

This proves that any multiple collision between  $m$  fronts can be resolved by shifting the speed of at most  $m - 2$  fronts by  $\delta_\sigma$ . Furthermore, no front will ever get its speed shifted more than once.  $\square$

By construction, exactly two fronts interact at each interaction point  $(x_n, \tau_n)$  using the front-tracking algorithm described above. The interaction points are isolated, however, we might have several interaction points at the same time  $t = \tau_n$ . For simplicity, we assume that there is only one interaction point for each time, so that we have a sequence of collision times  $\tau_1 < \tau_2 < \dots$ . Front tracking yields a piecewise constant function  $U^\delta(\cdot, t)$  defined for all  $t \leq \lim_{n \rightarrow \infty} \tau_n$ . We shall show that either  $\{\tau_n\}$  is a finite sequence or  $\lim_{n \rightarrow \infty} \tau_n = \infty$ , i.e., that  $U^\delta(\cdot, t)$  can be constructed for any  $t > 0$ .

Before we turn to the interaction estimates, we look at the error introduced using the simplified solver instead of the approximate solver. The lemma is given for the interactions involving a 1-front, but we have the same results for the symmetric interactions involving a 3-front.

**Lemma 3.3.** *Consider the interaction  $\zeta + \epsilon$ . Let*

$$\zeta + \epsilon \rightarrow \hat{\epsilon} + \zeta + \hat{\eta},$$

*be the solution obtained using the approximate solver, with intermediate states  $\hat{U}_i$ ,  $i = 1, 2$ , and let*

$$\zeta + \epsilon \rightarrow \epsilon' + \zeta + \theta^{np},$$

*be the solution obtained using the simplified solver, with intermediate states  $\tilde{U}_i$ ,  $i = 1, 2$ . Then,*

$$\begin{aligned} |\sigma_{\hat{\alpha}} - \sigma_{\alpha'}| &= \mathcal{O}(1) |\theta^{np}|, & \text{if } \epsilon' = \alpha', \\ |\lambda_{\hat{\mu}} - \lambda_{\mu'}| &= 0, & \text{if } \epsilon' = \mu'. \end{aligned}$$

Moreover,  $|\hat{U}_i - \tilde{U}_i| = \mathcal{O}(1) |\theta^{np}|$ ,  $i = 1, 2$ , and  $|U_r - \tilde{U}_2| = \mathcal{O}(1) |\theta^{np}|$ .

*Proof.* First note that  $p$  and  $u$  are equal for  $\tilde{U}_1$  and  $\tilde{U}_2$ , and for  $\hat{U}_1$  and  $\hat{U}_2$ , and we therefore omit the indices. Figure 4 shows the solutions of  $\zeta + \epsilon$  using both the

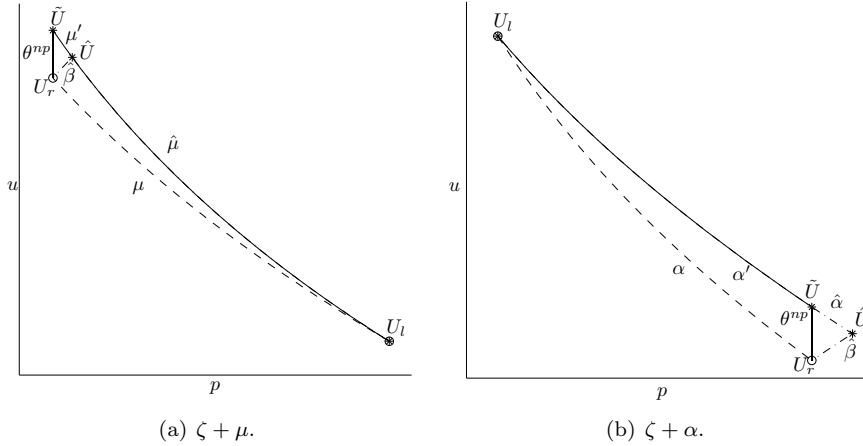


FIGURE 4. The interaction (dashed lines) solved by the approximate solver (dash-dotted lines) and by the simplified solver (solid lines).

approximate and simplified solver for the case with  $\hat{\eta} = \hat{\beta}$ . The rarefaction fronts  $\mu'$  and  $\hat{\mu}$  have the same left state, and they therefore have the same speed. Likewise, the left state is the same for  $\alpha'$  and  $\hat{\alpha}$ . However, the speed of a shock-front depends on the value of  $p$  at the right state as well, where  $p = \tilde{p}$  for  $\alpha'$  and  $p = \hat{p}$  for  $\hat{\alpha}$ . Since this difference in  $p$  is less than a constant times the jump in  $u$  across the non-physical front, that is,  $|\tilde{p} - \hat{p}| = \mathcal{O}(1) |\theta^{np}|$ , we get

$$|\sigma_{\hat{\alpha}} - \sigma_{\alpha'}| = |\sigma_1(p_l, \hat{p}) - \sigma_1(p_l, \tilde{p})| \leq |\sigma'_1(p_l, p^*)| |\tilde{p} - \hat{p}| = \mathcal{O}(1) |\theta^{np}|,$$

where  $\sigma'_1$  is the derivative with respect to the second argument and  $\hat{p} \leq p^* \leq \tilde{p}$ .

Moreover,  $\gamma$  is equal for the two solutions and  $|\tilde{u} - \hat{u}| \leq |\theta^{np}|$ , thus,  $|\hat{U}_i - \tilde{U}_i| = \mathcal{O}(1) |\theta^{np}|$ ,  $i = 1, 2$ . Furthermore,  $\tilde{p}_2 = p_r$  and  $|\tilde{u}_2 - u_r| = |\theta^{np}|$ , hence,  $|U_r - \tilde{U}_2| = \mathcal{O}(1) |\theta^{np}|$ .  $\square$

**3.2. The decreasing Glimm functional.** Define *time lines* as  $t_n = (\tau_n + \tau_{n+1})/2$ , where  $\tau_0 = 0$  by definition, and define the functional

$$(3.2) \quad G(t_n) := F_1(t_n) + \frac{1}{2}F_2(t_n) + kF_3(t_n) \\ + C_1(\bar{\gamma} - 1)(3Q_1(t_n) + Q_2(t_n)) + 3C_2Q_3(t_n),$$

where  $C_1$  is the constant appearing in the estimates given by (3.19) for the interaction of Type Baa, cf. the proof of Proposition 3.5,

$$(3.3) \quad C_2 := \frac{c_2}{\min\{r'_{\min}, s'_{\min}\}} = kc_2,$$

where  $c_2$  is the constant from Lemma 2.2 and

$$(3.4) \quad k := \frac{1}{\min\{r'_{\min}, s'_{\min}\}}.$$

Note that both  $C_1$  and  $C_2$  are constants only depending on  $p_{\min}$ ,  $p_{\max}$  and  $\bar{\gamma}$ . The linear functionals  $F_i$  and the quadratic functionals  $Q_i$  are defined by

$$(3.5) \quad F_1(t_n) := \sum\{|\theta| \mid \text{all shock-fronts } \theta \text{ at } t = t_n\},$$

$$(3.6) \quad F_2(t_n) := \sum\{|\theta| \mid \text{all rarefaction-fronts } \theta \text{ at } t = t_n\},$$

$$(3.7) \quad F_3(t_n) := \sum\{|\theta^{\text{np}}| \mid \text{all non-physical fronts at } t = t_n\},$$

$$(3.8) \quad Q_1(t_n) := \sum\{|\alpha||\beta| \mid \text{all } \alpha, \beta \in \mathcal{A}(t_n)\},$$

$$(3.9) \quad Q_2(t_n) := \sum\{|\epsilon||\eta| \mid \text{all } \epsilon \text{ and } \eta \text{ of different types in } \mathcal{A}(t_n)\},$$

$$(3.10) \quad Q_3(t_n) := \sum\{|\zeta||\theta| \mid \text{all } \zeta, \theta \in \mathcal{A}(t_n)\},$$

where  $\mathcal{A}(t)$  is the set of approaching fronts of different families at the time  $t$ . Note that two fronts of different families are approaching if the front of the lowest family is to the right of the other.

The functional (3.2) is an extension of the Glimm functional used in [14]. We have added linear terms summing over rarefaction- and non-physical fronts and  $Q_2$  summing over approaching rarefaction- and shock-fronts of different families.

**Remark 3.4.** The functional used in [14] for the Glimm scheme is decreasing in time for all possible interactions in the front-tracking algorithm as well. However, we need the extended functional (3.2) when estimating the total amount of non-physical fronts, cf. Section 3.4.

We need two more functionals defined as follows

$$(3.11) \quad L(t_n) := F_1(t_n) + F_2(t_n) + F_3(t_n),$$

$$(3.12) \quad F_\gamma := \sum\{|\zeta| \mid \text{all } \zeta\}.$$

Note that the sum of all contact discontinuities,  $F_\gamma$ , is constant for all time lines and that  $L(t_0) = F_1(t_0) + F_2(t_0)$  since the first non-physical front is generated at some  $t > t_0$ .

Let

$$(3.13) \quad C = \min\{\tilde{C}, 1\},$$

where the minimum is taken over all the constants  $\tilde{C}$  appearing in the estimates for interactions of Type Ba discussed in the proof of Proposition 3.5. Note that  $0 < C \leq 1$  depends only on  $p_{\min}$ ,  $p_{\max}$  and  $\bar{\gamma}$ . We now prove that under some given conditions,  $G$  is a decreasing functional in time.

**Proposition 3.5.** *If*

$$(3.14) \quad C_1(\bar{\gamma} - 1)L(t_0) \leq \frac{C}{18} \quad \text{and} \quad C_2F_\gamma \leq \frac{C}{18},$$

*then  $G$  defined by (3.2) is decreasing and*

$$(3.15) \quad F_1(t_n) + \frac{1}{2}F_2(t_n) + kF_3(t_n) \leq \frac{4}{3}L(t_0).$$

While proving this proposition, we will also obtain additional results for some particular types of interactions which we have collected in Corollary 3.6. By a *new rarefaction-collision* we mean an interaction where there is an outgoing rarefaction wave  $\theta'$  of a family in which there are no incoming rarefaction-fronts. Furthermore, an *increasing rarefaction-collision* refers to an interaction where the strength of an outgoing rarefaction wave is greater than the strength of the incoming rarefaction-front of the same family by an amount  $q > 0$ . Note that the  $\gamma$ -collisions, that is, the interactions involving a contact discontinuity, can also be new rarefaction-collisions, increasing rarefaction-collisions, or even both.

**Corollary 3.6.** *If condition (3.14) is satisfied, then  $G$  is strictly decreasing for all  $\gamma$ -collisions and for all interactions between two fronts of the same family. In particular,  $G$  decreases by at least*

- (i)  $\frac{1}{4}q$  across an increasing rarefaction-collision.
- (ii)  $\frac{1}{4}|\theta'|$  across a new rarefaction-collision.
- (iii)  $\frac{1}{2}|\theta||\zeta|$  across a  $\gamma$ -collision.
- (iv)  $2k|\theta^{np}|$  across an interaction generating a non-physical front  $\theta^{np}$ . Furthermore,  $|\theta^{np}| \leq c_2\rho$  for any non-physical front.

*Proof of Proposition 3.5.* The proof is based on induction on successive time lines: First we show that  $G(t_1) - G(t_0) \leq 0$ . Then we assume  $G(t_n) \leq G(t_{n-1}) \leq \dots \leq G(t_0)$ . The induction step is to show that  $\Delta G := G(t_{n+1}) - G(t_n) \leq 0$ . We only give the estimates for  $\Delta G$  here. Estimating  $G(t_1) - G(t_0)$  is very similar, giving terms involving  $L(t_0)$  where the estimate for  $\Delta G$  has terms involving  $L(t_n)$ . Note that if  $G$  is decreasing for all  $t \leq t_n$ , then we have

$$(3.16) \quad \begin{aligned} F_1(t_n) + \frac{1}{2}F_2(t_n) + kF_3(t_n) &\leq G(t_n) \leq \dots \leq G(t_0) \\ &= F_1(t_0) + \frac{1}{2}F_2(t_0) + C_1(\bar{\gamma} - 1)(3Q_1(t_0) + Q_2(t_0)) + 3C_2Q_3(t_0) \\ &\leq L(t_0) + C_1(\bar{\gamma} - 1)F_1(t_0)(3F_1(t_0) + F_2(t_0)) + 3C_2L(t_0)F_\gamma \\ &\leq (1 + 3C_1(\bar{\gamma} - 1)F_1(t_0) + 3C_2F_\gamma)L(t_0) \\ &\leq (1 + 3C_1(\bar{\gamma} - 1)L(t_0) + 3C_2F_\gamma)L(t_0) \\ &\leq \left(1 + \frac{C}{6} + \frac{C}{6}\right)L(t_0) \leq \frac{4}{3}L(t_0), \end{aligned}$$

where we used that  $F_3(t_0) = 0$ .

By construction, there is only one interaction between two successive time lines and we show that  $G$  decreases across all interactions. The interactions with no incoming non-physical fronts are the same as the interactions between two fronts in the Glimm scheme, cf. [14], and we therefore label the interactions in the same manner as in [14]. All the estimates for interactions without a contact discontinuity are obtained from the estimates by Nishida and Smoller in [19], while the estimates for interactions with a contact discontinuity are found using Lemma 2.2. We state only the estimates here, see [14] for more details.

Type Ba: Two waves of the same family.

- (i)  $\alpha_1 + \alpha_2 \rightarrow \alpha' + \nu'$ , shown in Figure 5, symmetric to  $\beta_1 + \beta_2 \rightarrow \mu' + \beta'$ : This is a new rarefaction-collision and we have

$$|\alpha'| - |\alpha_1| - |\alpha_2| = -|\nu'| \Rightarrow \Delta G \leq -\frac{7}{27} |\nu'| \leq -\frac{1}{4} |\nu'|.$$

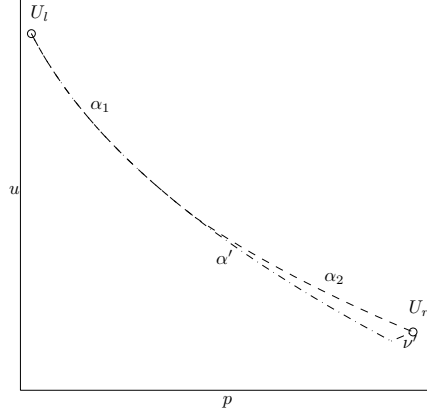


FIGURE 5. The interaction  $\alpha_1 + \alpha_2 \rightarrow \alpha' + \nu'$ .

- (ii)  $\alpha + \mu$ , symmetric to  $\nu + \beta$ . There are two possible outcomes, as shown in Figure 6:

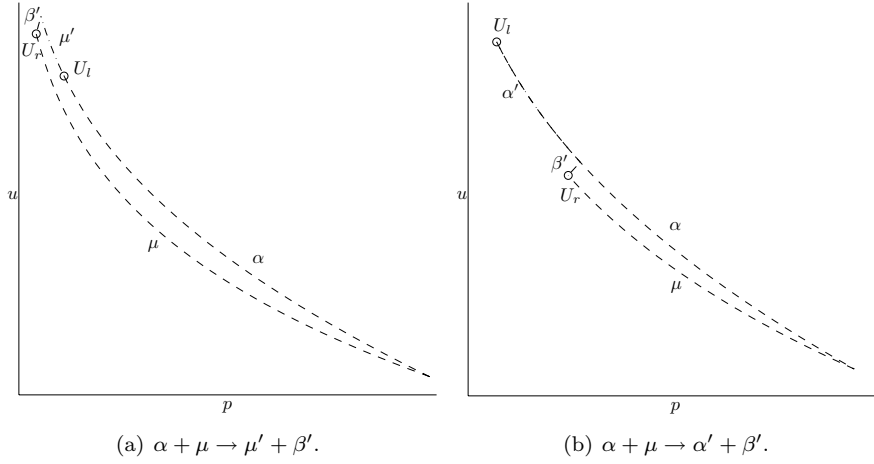


FIGURE 6. The interaction  $\alpha + \mu$ .

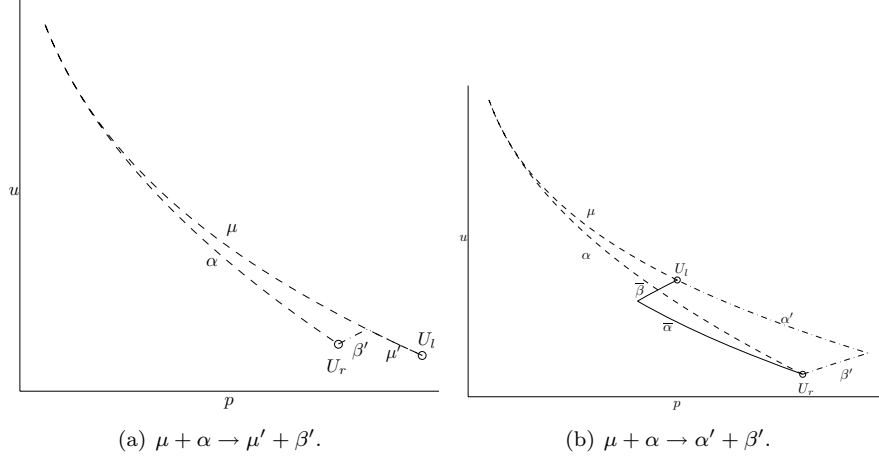
- $\alpha + \mu \rightarrow \mu' + \beta'$ : For this case we have

$$|\mu'| \leq |\mu|, |\beta'| - |\alpha| \leq -\tilde{C} |\beta'| \Rightarrow \Delta G < 0.$$

- $\alpha + \mu \rightarrow \alpha' + \beta'$ : We have

$$|\alpha'| + |\beta'| - |\alpha| \leq -\tilde{C} |\beta'| \Rightarrow \Delta G < 0.$$

- (iii)  $\mu + \alpha$ , symmetric to  $\beta + \nu$ : There are two possible outcomes, as shown in Figure 7:

FIGURE 7. The interaction  $\mu + \alpha$ .

- $\mu + \alpha \rightarrow \mu' + \beta'$ : For this case

$$|\mu'| \leq |\mu|, |\beta'| - |\alpha| \leq -\tilde{C}|\beta'| \Rightarrow \Delta G < 0.$$

- $\mu + \alpha \rightarrow \alpha' + \beta'$ . In this case, the interaction is replaced by a new one, see Figure 7(b),

$$(3.17) \quad \mu + \alpha \xrightarrow{\Delta G_1} \bar{\beta} + \bar{\alpha} \xrightarrow{\Delta G_2} \alpha' + \beta',$$

for which we have the estimate

$$|\bar{\alpha}| + |\bar{\beta}| - |\alpha| \leq -\tilde{C}|\bar{\beta}| \Rightarrow \Delta G_1 < 0.$$

Furthermore, we have  $\Delta G_2 \leq 0$  by estimate (3.19) for  $\beta + \alpha$  below, cf. Type Bii. Hence,  $\Delta G \leq 0$ .

*Type Bb: Different families, no contact discontinuity.*

- (i)  $\nu + \mu \rightarrow \mu' + \nu'$ , as shown in Figure 8(a). None of the rarefaction-fronts increase, and we have

$$(3.18) \quad |\mu'| \leq |\mu|, |\nu'| \leq |\nu| \Rightarrow \Delta G_1 \leq 0.$$

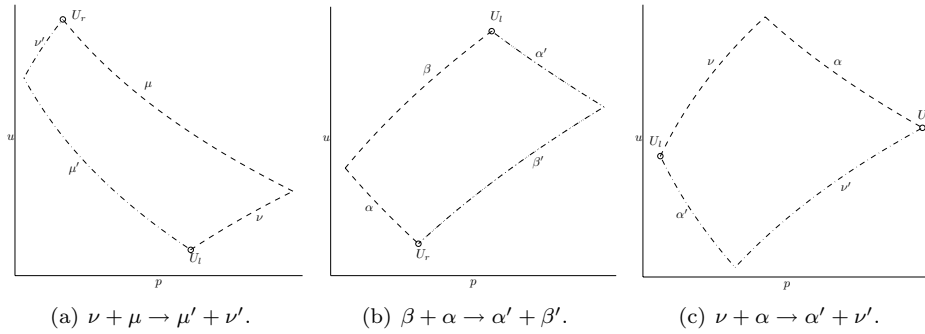


FIGURE 8. The interactions of Type Bb

(ii)  $\beta + \alpha \rightarrow \alpha' + \beta'$ , as shown in Figure 8(b). We have

$$(3.19) \quad |\alpha'| - |\alpha| \leq (\bar{\gamma} - 1)C_1 |\alpha| |\beta|, \quad |\beta'| - |\beta| \leq (\bar{\gamma} - 1)C_1 |\alpha| |\beta|,$$

thus

$$\Delta G \leq -\frac{1}{9}(\bar{\gamma} - 1)C_1 |\alpha| |\beta| < 0.$$

(iii)  $\nu + \alpha \rightarrow \alpha' + \nu'$ , as shown in Figure 8(c), symmetric to  $\beta + \mu \rightarrow \mu' + \beta'$ . This is an increasing rarefaction-collision where we for  $q = |\nu'| - |\nu| \geq 0$  have

$$(3.20) \quad |\alpha'| - |\alpha| = -q, \quad |\nu'| - |\nu| \leq q \Rightarrow \Delta G \leq -\frac{1}{4}q.$$

*Type Bc: With a contact discontinuity.* These are the four possible  $\gamma$ -collisions.

(i)  $\zeta + \mu$ , symmetric to  $\nu + \zeta$ : For this  $\gamma$ -collision there are two outcomes where all fronts are physical, see Figure 9, and one outcome generating a non-physical front as shown in Figure 10(a).

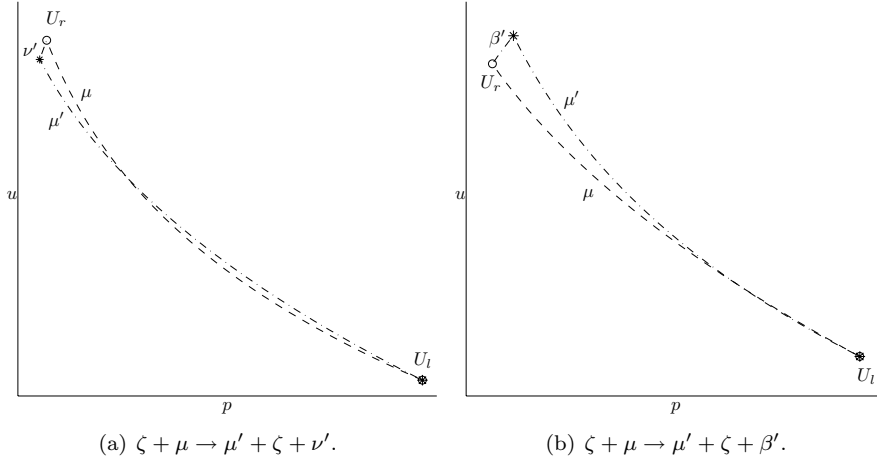


FIGURE 9. The interaction  $\zeta + \mu$ .

- $\zeta + \mu \rightarrow \mu' + \zeta + \nu'$ : This interaction is a new rarefaction-collision and an increasing rarefaction-collision with  $q = |\nu'|$ . We have

$$|\mu'| - |\mu| = |\nu'| \leq C_2 |\mu| |\zeta|,$$

from which we find

$$\Delta G \leq -2C_2 |\mu| |\zeta| \leq -\frac{1}{4} |\nu'| - \frac{1}{4} q.$$

- $\zeta + \mu \rightarrow \mu' + \zeta + \beta'$ : The rarefaction-front does not increase and

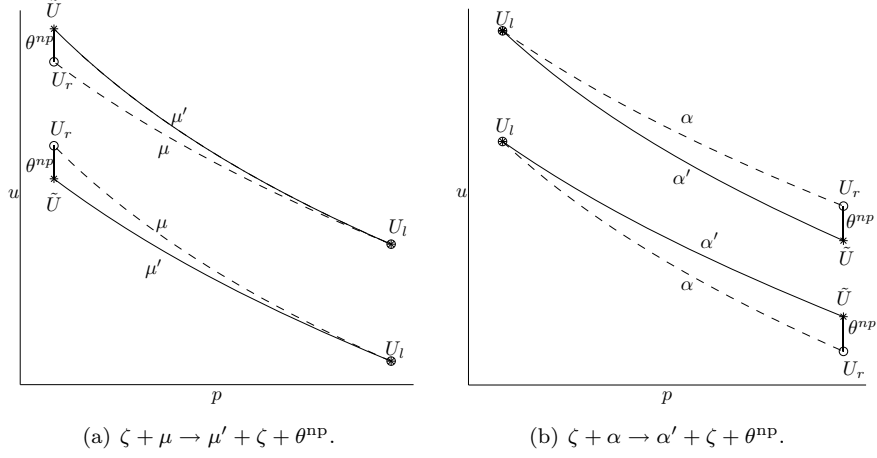
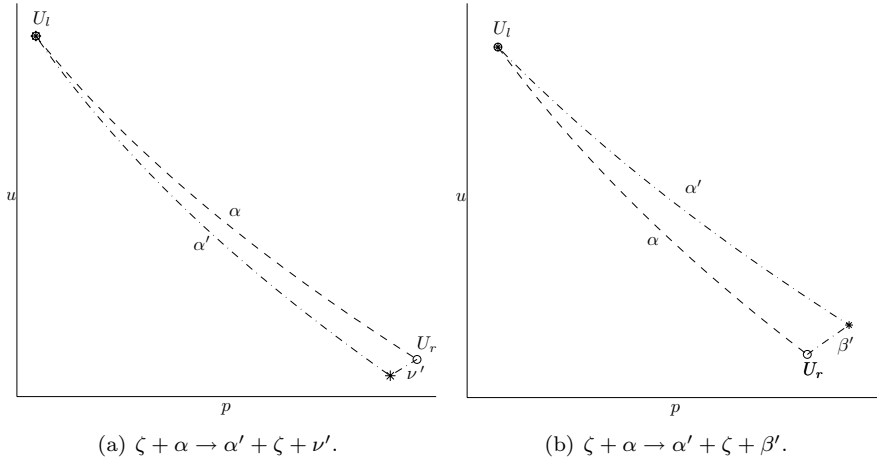
$$|\mu'| - |\mu| \leq 0, \quad |\beta'| \leq C_2 |\mu| |\zeta| \Rightarrow \Delta G \leq -C_2 |\mu| |\zeta|.$$

- $\zeta + \mu \rightarrow \mu' + \zeta + \theta^{\text{np}}$ : By construction,  $|\mu'| = |\mu|$ . Using Lemma 2.2, we find

$$|\theta^{\text{np}}| \leq c_2 |\mu| |\zeta| \Rightarrow \Delta G \leq -2C_2 |\mu| |\zeta| \leq -2k |\theta^{\text{np}}|,$$

since  $C_2 = kc_2$ , cf. (3.3), where  $k$  given by (3.4) depends only on  $p_{\min}$ ,  $p_{\max}$  and  $\bar{\gamma}$ .

(ii)  $\zeta + \alpha$ , symmetric to  $\beta + \zeta$ . This  $\gamma$ -collision has two possible outcomes where all fronts are physical, see Figure 11, and one outcome generating a non-physical front as shown in Figure 10(b).

FIGURE 10. Interactions of the type  $\zeta + \epsilon$  solved by the simplified solver.FIGURE 11. The interaction  $\zeta + \alpha$ .

- $\zeta + \alpha \rightarrow \alpha' + \zeta + \nu'$ : For this new rarefaction-collision we have

$$|\alpha'| - |\alpha| \leq 0, \quad |\nu'| \leq C_2 |\alpha| |\zeta|,$$

thus,

$$\Delta G \leq -2C_2 |\alpha| |\zeta| \leq -\frac{1}{4} |\nu'|.$$

- $\zeta + \alpha \rightarrow \alpha' + \zeta + \beta'$ : For this case we have

$$|\alpha'| - |\alpha| = |\beta'| \leq C_2 |\alpha| |\zeta| \Rightarrow \Delta G \leq -\frac{1}{2} C_2 |\zeta| |\beta'|.$$

- $\zeta + \alpha \rightarrow \alpha' + \zeta + \theta^{np}$ : By construction,  $|\alpha'| = |\alpha|$  and by Lemma 2.2

$$|\theta^{np}| \leq c_2 |\mu| |\zeta|. \Rightarrow \Delta G \leq -2C_2 |\alpha| |\zeta| \leq -2k |\theta^{np}|,$$

since  $C_2 = kc_2$ , where  $k$  only depends on  $p_{\min}$ ,  $p_{\max}$  and  $\bar{\gamma}$ .

Observe that for all  $\gamma$ -collision solved by the simplified solver we have  $|\theta^{np}| \leq c_2 |\theta| |\zeta|$ . Since the simplified solver is only used on  $\gamma$ -interactions satisfying (3.1), we therefore get  $|\theta^{np}| \leq c_2 \rho$  for any non-physical fronts.

The only interactions we have not covered yet, are interactions with incoming non-physical fronts. Neither the strength or type of the fronts change across these interactions, there is only a shift in  $u$  for which all wave curves are invariant. Hence,  $G$  is unchanged across these interactions. Note that this also applies to the case where two non-physical fronts interact, one traveling to the left and the other to the right.  $\square$

The following additional estimates for two of the interactions will be needed in Section 3.4.

**Lemma 3.7** (Additional estimates for interactions of Type Bai and Type Bbiii).

- (i) For  $\alpha_1 + \alpha_2 \rightarrow \alpha' + \nu'$  we have  $|\nu'| \leq \frac{29}{27} |\alpha_1|$ .
- (ii) For  $\nu + \alpha \rightarrow \alpha' + \nu'$  we have  $|\nu'| - |\nu| \leq C_1(\bar{\gamma} - 1) |\alpha| |\nu|$ .

*Proof.* We start with the quadratic estimate in (ii). This follows by the estimates for the shock curves discussed in [19] using the Riemann invariants. In the same manner as for the interaction between two shock curves of different families, cf. Type Bbii, we transfer the estimates to physical variables measuring the strengths in  $p$ , and then take the supremum over  $\gamma$ . Thus, the constant  $C_1$  is only dependent on  $p_{\min}$ ,  $p_{\max}$  and  $\bar{\gamma}$ , just as for the interaction between two shocks of different families.

We will use this quadratic estimate to prove the estimate in (i). Let  $\alpha_1 + \alpha_2$  connect  $U_l$  to  $U_r$  with  $U_0$  as the middle state. Consider the 3-rarefaction wave  $\bar{\nu}$  starting at  $U_l$  as depicted in Figure 12. Our first goal is to find a 1-shock wave

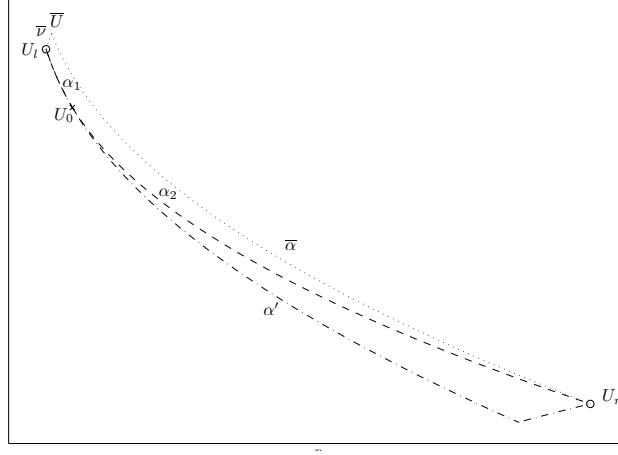


FIGURE 12. The setup for proving additional estimates for  $\alpha_1 + \alpha_2$ .

$\bar{\alpha}$  starting at a point  $\bar{U}$  on  $\bar{\nu}$  so that  $\bar{\nu} + \bar{\alpha}$  connects  $U_l$  to  $U_r$ . We know that if  $\bar{p} = p_0$ , then  $\bar{\alpha}$  will have the same slope as  $\alpha_2$ , hence, lies above  $\alpha_2$  and never reaches  $U_r$ . Likewise, if  $\bar{p} = p_l$ ,  $\bar{\alpha}$  will coincide with  $\alpha'$ , thus, lies below  $\alpha_2$  and never reaches  $U_r$ . By continuity of the shock curves, it then follows that there is a  $\bar{U}$ , with  $p_l < \bar{p} < p_0$ , so that  $\bar{\nu} + \bar{\alpha}$  connects  $U_l$  to  $U_r$  with  $\bar{U}$  as the intermediate state. In particular, we have that

$$|\bar{\alpha}| = p_r - \bar{p} \leq |\alpha_1| + |\alpha_2|, \quad |\bar{\nu}| = \bar{p} - p_l \leq p_0 - p_l = |\alpha_1|.$$

Furthermore,  $\bar{\nu} + \bar{\alpha} \rightarrow \alpha' + \nu'$ , and by using the estimates from (ii) we get

$$\begin{aligned} |\nu'| - |\alpha_1| &\leq |\nu'| - |\bar{\nu}| \leq C_1(\bar{\gamma} - 1) |\bar{\alpha}| |\bar{\nu}| \\ &\leq C_1(\bar{\gamma} - 1)(|\alpha_1| + |\alpha_2|) |\alpha_1| \leq C_1(\bar{\gamma} - 1) F_1(t_n) |\alpha_1| \\ &\leq C_1(\bar{\gamma} - 1) \frac{4}{3} L(t_0) |\alpha_1| \leq \frac{2}{27} |\alpha_1|. \end{aligned}$$

Hence,  $|\nu'| \leq \frac{29}{27}$ .  $\square$

**3.3. Finite number of interactions.** The next step is to show that the front-tracking algorithm generates an approximate solution in a finite number of steps. We do this by proving that there is a finite number of physical and non-physical fronts, and, hence, a finite number of interactions.

Firstly, recall that the solution of a Riemann problem consists of up to three waves, one from each family. However, an outgoing contact is only present if there is an incoming contact discontinuity. Thus, all interactions not a  $\gamma$ -collision have at most two outgoing waves and, hence, the number of fronts can only increase due to splitting of rarefaction waves. Likewise, the number of physical fronts only increases due to splitting of rarefaction waves for any  $\gamma$ -collision solved by the simplified solver, since these only have two physical outgoing waves. The interactions that might result in a split rarefaction wave are either a new rarefaction-collision or an increasing rarefaction-collision as defined in Section 3.1, and there is a finite number of such interactions.

**Lemma 3.8.** *For a fixed  $\delta$ , there is only a finite number of new rarefaction-collisions where the new rarefaction wave splits into two or more fronts.*

*Proof.* Let  $\theta'$  be the new outgoing rarefaction wave of a new rarefaction-collision. It will only split if its strength,  $|\theta'|$ , is larger than  $\delta$ . Moreover, from Corollary 3.6 we have  $\Delta G \leq -\frac{1}{4} |\theta'|$ . Hence,  $\Delta G \leq -\frac{1}{4} \delta$  across a new rarefaction-collision where the new rarefaction wave splits. Since  $G$  is a decreasing, non-negative functional, there can only be a finite number of interactions where  $G$  decreases by at least  $\frac{1}{4} \delta$ . This proves the lemma.  $\square$

We next consider increasing rarefaction-collisions and look at how  $G$  changes from a split rarefaction-front appears until it has gained enough strength to split again. That is, consider an increasing rarefaction-collision at  $t = \tau_1$  where the outgoing rarefaction wave splits into several fronts. Let  $\tau_n$  be the collision time when the first of the split rarefaction-fronts splits again after gaining strength through one or more increasing rarefaction-collisions. Fix two time lines,  $t_i$  and  $t_j$ , so that  $t_i < \tau_1 < \tau_n < t_j$ . Assume that the only rarefaction-front crossing  $t = t_i$  that results in a split rarefaction wave before  $t = t_j$ , is the rarefaction-front colliding at  $t = \tau_1$ . Define  $\Delta G_{\text{split}} := G(t_j) - G(t_i)$ .

**Lemma 3.9.** *Let  $t_i < \tau_1 < \tau_n < t_j$  and  $\Delta G_{\text{split}}$  be as defined above. Then, for a fixed  $\delta$ ,*

$$(3.21) \quad \Delta G_{\text{split}} \leq -\frac{1}{8} \delta.$$

*Furthermore, there is only a finite number of increasing rarefaction-collisions where the increasing rarefaction wave splits into two or more fronts.*

*Proof.* From Corollary 3.6 we have  $\Delta G \leq -\frac{1}{4} q$  for all increasing rarefaction-collisions where  $q > 0$  is the increase, that is, the strength of the outgoing rarefaction wave is less than or equal to  $q$  plus the strength of the incoming rarefaction-front of the same family. Let  $\theta'$  be the outgoing rarefaction wave of the increasing rarefaction-collision

at  $t = \tau_1$ , thus,  $\theta'$  splits, and let furthermore  $\theta_0$  be the incoming rarefaction-front of the same family. By the assumptions,  $|\theta_0| = a\delta$  for  $0 < a \leq 1$ , and

$$\delta < |\theta'| \leq |\theta_0| + q_1.$$

Furthermore,  $\Delta G_1 \leq -\frac{1}{4}q_1$  across this interaction. Let  $m$  be the number of fronts  $\theta'$  splits into and let furthermore  $\theta_1$  denote the split front that leads to the first front splitting again. Thus,

$$|\theta_1| = \frac{1}{m} |\theta'| \leq \frac{|\theta_0| + q_1}{m} = \frac{a\delta + q_1}{m}.$$

We follow this path of rarefaction-fronts until the rarefaction wave  $\theta_n$  splits after an

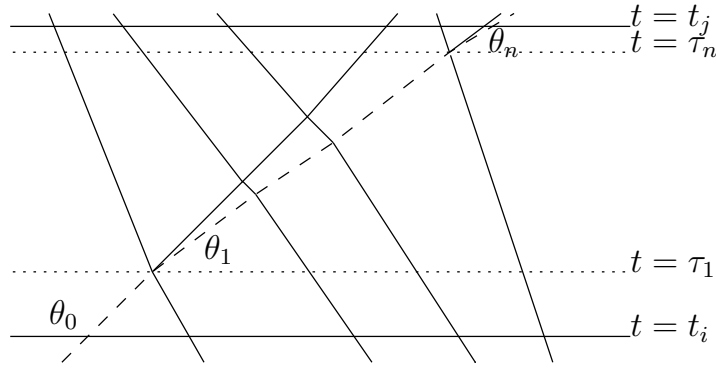


FIGURE 13. An illustration of several increasing rarefaction-collisions where a rarefaction wave splits at  $t = \tau_1$  and  $t = \tau_n$ .

interaction at  $t = \tau_n$ . In Figure 13, where  $m = 2$ , the path is drawn by dashed lines. The only way the rarefaction-front gains strength is through increasing rarefaction-collisions, all other interactions only weaken the rarefaction-front. We can therefore assume that the rarefaction-front we follow is only involved in increasing rarefaction-collisions up to  $t = t_j$ . For each interaction the strength of the rarefaction-front increases by at most  $q_i$ , thus,

$$(3.22) \quad |\theta_n| \leq |\theta_{n-1}| + q_n \leq |\theta_1| + \sum_2^n q_k \leq \frac{a\delta + q_1}{m} + \sum_2^n q_k \leq \frac{a}{m}\delta + \sum_1^n q_k,$$

and  $\Delta G_k \leq -\frac{1}{4}q_k$  for  $k = 1, \dots, n$ . By definition,  $\tau_n$  is the first collision time after  $\tau_1$  where a rarefaction wave splits, thus,

$$(3.23) \quad |\theta_{n-1}| \leq \delta < |\theta_n|.$$

All interactions taking place between  $t_i$  and  $t_j$  have  $\Delta G \leq 0$  by Proposition 3.5. Summing over these, and combining (3.22) and (3.23) we get

$$\begin{aligned} \Delta G_{\text{split}} &= \sum_{\tau_k} \Delta G(\tau_k) + \sum_{\tau \neq \tau_k} \Delta G(\tau) \leq \sum_{\tau_k} \Delta G(\tau_k) \\ &\leq \sum_{i=1}^n -\frac{1}{4}q_k \leq -\frac{1}{4} \left(1 - \frac{a}{m}\right) \delta \leq -\frac{1}{4} \cdot \frac{1}{2} \delta \leq -\frac{1}{8} \delta, \end{aligned}$$

where we have used that  $0 < a \leq 1$  and  $m \geq 2$ . This proves (3.21).

Furthermore,  $G$  is non-negative and decreases by at least  $\frac{1}{8}\delta$  from the time when a rarefaction wave splits due to an increasing rarefaction-collision until the time when the first of the split fronts has gained enough strength to split again. Hence, this

can only happen a finite number of times, and therefore, there can only be a finite number of increasing rarefaction-collisions where the rarefaction wave splits.  $\square$

Thus, by Lemma 3.8 and Lemma 3.9, there is a finite number of interactions resulting in split rarefaction waves. That is, there is only a finite number of interactions with more than one outgoing front of each family.

Except for split rarefaction waves, the number of fronts increases only for the  $\gamma$ -collisions solved by the approximate solver, that is, interactions with  $|\theta||\zeta| > \rho$ , where  $\theta$  is the incoming 1- or 3-front. These interactions have at least three outgoing physical fronts. By Proposition 3.5,  $G$  decreases and, in particular,  $\Delta G \leq 0$  for all interactions. Therefore,

$$0 < G(t_n) \leq G(t_0) + \sum_{\tau < t_n} \Delta G(\tau) \leq G(t_0) + \sum_{\tau_\gamma < t_n} \Delta G(\tau_\gamma),$$

where  $\tau$  is any collision time and  $\tau_\gamma$  is the collision time of a  $\gamma$ -collision solved by the approximate solver. Furthermore, Corollary 3.6 states that  $\Delta G \leq -\frac{1}{2}|\theta||\zeta|$  for all  $\gamma$ -collisions, thus,

$$\sum_{\tau_\gamma < t_n} |\theta||\zeta| \leq -2 \sum_{\tau_\gamma < t_n} \Delta G(\tau_\gamma) \leq 2G(t_0).$$

This estimate is true for all  $t_n < \infty$ , hence, there is at most  $2G(t_0)/\rho$  number of  $\gamma$ -collisions where  $|\theta||\zeta| > \rho$ , that is, where a  $\gamma$ -collision is solved by the approximate solver. These are the only interactions creating more physical fronts in addition to the finite number of split rarefaction waves. Thus, the number of physical fronts remains finite for all times. Moreover, non-physical fronts are only generated when physical fronts interact with a contact discontinuity. Each physical front can only interact once with a given contact discontinuity, and there is a finite number of contact discontinuities, hence, there is a finite number of interactions generating non-physical fronts.

In other words, there is a finite number of physical and non-physical fronts for any given time, and these fronts can only interact a finite number of times. Thus, front tracking gives us an approximate solution in a finite number of steps for any  $t \in (0, \infty)$ .

**3.4. The total amount of non-physical fronts.** In order to prove that the sequence of approximate solutions converges to a weak solution, we need to estimate the total amount of non-physical fronts introduced.

First of all, we assign *generations* to all fronts except the contact discontinuities. All initial 1- and 3-fronts are of generation one. Whenever two fronts interact, the outgoing fronts are assigned the same generation as the lowest generation of the incoming fronts of the same family. If there is no incoming front of the same family, the outgoing front is assigned a generation one higher than the highest generation of the incoming fronts. Note that the contact discontinuities have no generation assigned to them. Furthermore, for any interaction with an incoming non-physical front, the outgoing fronts have the same generation, as well as strength and type, as the incoming ones. The above way to define generations agrees with the standard way, thus, the arguments of Bressan in [4] regarding the number of fronts of a given generation hold for our setting as well.

We proceed in a similar fashion as done in [1] and define a functional which correspond to (3.2) restricted to fronts of a given generation,

$$(3.24) \quad G_n = F_{1,n} + \frac{1}{2}F_{2,n} + kF_{3,n} + C_1(\bar{\gamma} - 1)(3Q_{1,n} + Q_{2,n}) + 3C_2Q_{3,n},$$

where  $F_{i,n}$  is defined by restricting the sums in (3.5)-(3.7) to fronts of generation  $n$ , while for  $Q_{i,n}$  we restrict the sums in (3.8)-(3.10) to approaching fronts where

the front of highest generation is of generation  $n$ . Let furthermore

$$(3.25) \quad \tilde{G}_n = \sum_{i \geq n} G_i.$$

Our goal is to estimate  $\sum_{i \geq k} \sum_{t=t_n} |\theta_i^{\text{np}}|$ , where  $\theta_i^{\text{np}}$  denotes a non-physical front of generation  $i$ , by obtaining estimates on  $\tilde{G}_k$ .

Let the generations of the two incoming fronts be denoted by  $m$  and  $h$  where  $m \leq h$ . For  $\gamma$ -collisions, where only one incoming front has a generation assigned, we let  $h = m$ . Furthermore, let  $\mathcal{T}_h$  denote the set of all interaction times  $\tau$  where the highest incoming generation is  $h$ . Moreover, we let  $[x]_- = \max\{-x, 0\}$  and  $[x]_+ = \max\{x, 0\}$ . Next, we estimate how  $G_n$  and  $\tilde{G}_n$  change across interactions.

**Lemma 3.10.** *Consider an interaction at the time  $\tau \in \mathcal{T}_h$ . There exists an  $\omega < 1$  so that:*

(i) *If  $k \geq h + 2$ , then  $\Delta \tilde{G}_k = \Delta G_k = 0$ .*

(ii) *If  $k = h + 1$ , then  $\Delta \tilde{G}_k = \Delta G_k \geq 0$  and*

$$(3.26) \quad \left[ \Delta \tilde{G}_k \right]_+ \leq \begin{cases} \omega [\Delta G_{k-1}]_-, & \text{if } h = m, \\ \omega ([\Delta G_{k-1}]_- - [\Delta G_m]_+), & \text{if } h > m. \end{cases}$$

(iii) *If  $h \geq k > m$ , then  $\Delta G_k \leq 0$  and  $\Delta \tilde{G}_k \leq 0$  with*

$$(3.27) \quad \left[ \Delta \tilde{G}_k \right]_- \geq [\Delta G_m]_+.$$

(iv) *If  $h \geq k = m$ , then  $\Delta \tilde{G}_k \leq 0$ . If  $h = k = m$ , then  $\Delta G_k \leq 0$ .*

(v) *If  $m > k$ , then  $\Delta G_k = 0$  and  $\Delta \tilde{G}_k \leq 0$ .*

*Proof.* First recall that for all interactions with an incoming non-physical front the outgoing fronts have the same type, strength and generation as the incoming ones. Therefore, these interactions have  $\Delta \tilde{G}_k = \Delta G_k = 0$  for all  $k$ , and we are left with considering interactions between two physical fronts.

Only fronts of generation  $m$ ,  $h$  and  $h + 1$  may be involved in a given interaction, hence,  $G_i = 0$  for all  $i \notin \{m, h, h + 1\}$ . From the way the sums in (3.24) are defined, and the interaction estimates given in Lemma 3.7(ii) and in the proof of Proposition 3.5, it follows that  $\Delta G_h \leq 0$  for all interactions.

(i) If  $k \geq h + 2$ , there are no fronts of generation  $k$  or higher involved in the interaction, hence,  $\Delta \tilde{G}_k = \Delta G_k = 0$ .

(ii) If  $k = h + 1$ , there are no fronts of generation  $k + 1$  or higher involved, hence,  $\Delta \tilde{G}_k = \Delta G_k$ . For interactions between a 3-front and a 1-front, there are no fronts of generation  $k = h + 1$  involved either, thus,  $\Delta G_k = 0$ . The other interactions generate fronts of generation  $k = h + 1$ , therefore  $\Delta G_k$  will be positive. Furthermore,  $\Delta G_{k-1} = \Delta G_h \leq 0$ , and from Corollary 3.6 we have  $\Delta G < 0$ . For the case  $m = h$  and the case  $h > m$  where  $\Delta G_m \geq 0$  it then follows that there exists an  $\omega < 1$  so that

$$\frac{1}{\omega} [\Delta G_k]_+ - [\Delta G_{k-1}]_- \leq 0,$$

$$\frac{1}{\omega} [\Delta G_k]_+ - [\Delta G_{k-1}]_- + [\Delta G_m]_+ \leq 0,$$

respectively, which proves estimate (3.26) for these cases. This includes all the  $\gamma$ -collisions, and the strongest condition we get is  $\omega \geq 25/29$ . However, for the last case where  $h > m$  and  $\Delta G_m \leq 0$ , the strictly decreasing  $G$  is not enough to obtain (3.26), and we have to calculate

$$(3.28) \quad \frac{1}{\omega} [\Delta G_k]_+ - [\Delta G_{k-1}]_-$$

for each interaction. Consider first the interactions between a shock- and a rarefaction-front of the same family. From the estimates in the proof of Proposition 3.5 it follows that (3.28) is less than zero if  $\omega \geq (1 + 7C/18)/(1 + C/2)$ . The last interaction of this case is the interaction between two shocks of the same family. Here, we have  $\Delta G_m \leq 0$  only if the rightmost shock,  $\alpha_2$ , has generation  $m$  and  $|\alpha'| \leq |\alpha_2|$ . Then,  $|\alpha_1| \leq |\nu'|$ , but according to our additional estimate in Lemma 3.7(i) we have  $|\nu'| \leq 29/27 |\alpha_1|$ . We thereby find that (3.28) is less than zero if  $\omega \geq 580/729$ . Hence, estimate (3.26) holds for all  $k = h + 1$  with

$$\omega = \max \left\{ \frac{25}{29}, \frac{1 + \frac{7}{18}C}{1 + \frac{1}{2}C} \right\} < 1.$$

- (iii) Consider first the case where  $k = h$  and recall that then  $\Delta G_k \leq 0$ . For an interaction between a 3- and a 1-front we have  $\Delta \tilde{G}_k = \Delta G_k \leq 0$ , thus, (3.27) follows from  $\Delta G_k + \Delta G_m = \Delta G \leq 0$ . For interactions generating fronts of generation  $h + 1$  we have  $\frac{1}{\omega} \Delta \tilde{G}_k \leq \frac{1}{\omega} [\Delta G_{h+1}]_+ - [\Delta G_h]_- \leq 0$ , where the last inequality follows from the above discussion. Since  $\Delta G \leq 0$  for these interactions, we therefore obtain (3.27). Because  $\Delta G_i = 0$  for all  $m < i < h$ , we have  $\Delta \tilde{G}_k = \Delta \tilde{G}_h$  for all  $h > k > m$ , hence, (3.27) follows.
- (iv) If  $k = m$ , then  $\Delta \tilde{G}_k = \Delta G \leq 0$  by Proposition 3.5. Furthermore, if  $k = h = m$ , then  $\Delta G_k = \Delta G \leq 0$ .
- (v) If  $k \leq m$ , then there are no fronts of generation  $k$  involved and  $\Delta G_k = 0$ . Moreover,  $\Delta \tilde{G}_k = \Delta G \leq 0$  by Proposition 3.5.

□

The signs of  $\Delta G_k$  and  $\Delta \tilde{G}_k$  are summarized in Table 1. Since  $\Delta G_i$  may be

	$k \geq h + 2$	$k = h + 1$	$h \geq k > m$	$h \geq k = m$	$m > k$
$\Delta G_k$	0	+	-	$\pm$	0
$\Delta \tilde{G}_k$	0	+	-	-	-

TABLE 1. Signs of  $\Delta G_k$  and  $\Delta \tilde{G}_k$ .

positive only for  $i = m$  and  $i = h + 1$ , we can rewrite (3.26) for  $k = h + 1$  as

$$\left[ \Delta \tilde{G}_k \right]_+ \leq \omega \left( [\Delta G_{k-1}]_- - \sum_{i=1}^{k-2} [\Delta G_i]_+ \right).$$

Moreover, rewriting (3.27) we get

$$\left[ \Delta \tilde{G}_k \right]_- \geq \sum_{i=1}^{k-1} [\Delta G_i]_+,$$

which is valid for all  $h \geq k$ . Thus, our estimates given in Lemma 3.10 are the same estimates as obtained in [1, Proposition 6.5] by Amadori and Corli (where  $F$  is used to denote the functional corresponding to our  $G$ ). The signs of  $\Delta G_k$  and  $\Delta \tilde{G}_k$  are also the same as the ones found in [1]. Hence, by the same proofs as presented in [1], we can establish the following result:

**Lemma 3.11** (Corresponds to Proposition 6.7 in [1]). *Assume (3.14) is satisfied, then*

$$(3.29) \quad \tilde{F}_{3,k}(t) \leq \tilde{G}_k(t) \leq \omega^{k-1} G(0).$$

Let  $N_j$  be the number of fronts of generation less than or equal to  $j$ , and note that this includes both the physical and non-physical fronts. From the previous section we know that  $N_j$  is finite, and according to [4, Ch. 7.3],

$$N_j \leq P_j(N_0, \delta^{-1}),$$

where  $P_j$  is a polynomial function of  $\delta^{-1}$  and the number of initial fronts,  $N_0$ . Using this, we can finally prove the following:

**Lemma 3.12.** *For any given  $\delta_{\text{init}} > 0$  there exists a threshold parameter  $\rho > 0$  so that*

$$\sum_{t=t_n} |\theta^{np}| = \mathcal{O}(\delta_{\text{init}}).$$

*Proof.* For a fixed number  $k$ , the number of non-physical fronts of generation less than or equal to  $k-1$  is less than  $N_{k-1}$ , which again is bounded by  $P_{k-1}(N_0, \delta^{-1})$ . Furthermore,  $|\theta^{np}| \leq c_2\rho$  by Corollary 3.6. Thus, using Lemma 3.11 and recalling that  $0 < \omega < 1$ , we get

$$\begin{aligned} \sum_t |\theta^{np}| &\leq \sum_t \sum_{i \leq k-1} |\theta_i^{np}|(t) + \tilde{F}_{3,k}(t) \\ &\leq c_2\rho P_{k-1}(N_0, \delta^{-1}) + \omega^{k-1}G(0) = \mathcal{O}(\delta_{\text{init}}), \end{aligned}$$

by choosing  $k$  so that  $\omega^{k-1} = \mathcal{O}(\delta_{\text{init}})$  and then  $\rho$  so that  $c_2\rho P_{j_0}(N_0, \delta^{-1}) = \mathcal{O}(\delta_{\text{init}})$ .  $\square$

**3.5. Bounded total variation.** We have established that if condition (3.14) is satisfied, then  $G$  is decreasing and  $U^\delta$  can be defined up to any time, as long as  $U^\delta$  is contained in some domain  $\mathcal{D}$  given by (2.17). The next step is to bound the total variation of  $U^\delta$ , and then show that such a domain  $\mathcal{D}$  exists.

From Section 3.2 we recall that  $C_1$  is the constant appearing in estimate (3.19),  $C_2$  is given by (3.3),  $k$  by (3.4), and  $C$  by (3.13). Define the constant

$$\kappa := \frac{8}{3}s'_{\max} + 1,$$

where  $s'_{\max}$  is the upper bound of  $\partial s / \partial p$ , cf. property (v) of Lemma 2.1. Given these constants, that only depend on  $p_{\min}$ ,  $p_{\max}$  and  $\bar{\gamma}$ , we can state the following result.

**Lemma 3.13.** *If the initial data satisfy*

$$(3.30) \quad (\bar{\gamma} - 1)\text{T.V.}(p_0, u_0) \leq \frac{C}{18kC_1} \quad \text{and} \quad \text{T.V.}(\gamma_0) \leq \frac{C}{18C_2},$$

*and the approximate solution  $U^\delta(x, t) = (p^\delta(x, t), u^\delta(x, t), \gamma^\delta(x, t))$  obtained using front tracking is bounded with  $p^\delta(x, t) \geq p_{\min} > 0$ , then*

$$(3.31) \quad \text{T.V.}(p^\delta(\cdot, t), u^\delta(\cdot, t)) \leq 2\kappa k \text{T.V.}(p_0, u_0),$$

$$(3.32) \quad \text{T.V.}(\gamma^\delta(\cdot, t)) \leq \text{T.V.}(\gamma_0).$$

*Proof.* Note that (3.32) is obvious since  $\gamma$  only changes along contact discontinuities, thus,

$$\text{T.V.}(\gamma^\delta(\cdot, t_n)) = F_\gamma = \text{T.V.}(\gamma^\delta(\cdot, 0)) \leq \text{T.V.}(\gamma_0),$$

for any time line  $t = t_n$ . Furthermore,

$$L(t_0) \leq \text{T.V.}(p^\delta(\cdot, 0)) + k \text{T.V.}(u^\delta(\cdot, 0)) \leq k \text{T.V.}(p^\delta(\cdot, 0), u^\delta(\cdot, 0)),$$

for  $t_0 = 0+$ . Whenever (3.30) is satisfied, we therefore have

$$\begin{aligned} C_1(\bar{\gamma} - 1)L(t_0) &\leq C_1(\bar{\gamma} - 1)k \text{T.V.}(p^\delta(\cdot, 0), u^\delta(\cdot, 0)) \\ &\leq C_1(\bar{\gamma} - 1)k \text{T.V.}(p_0, u_0) \leq \frac{C}{18}, \end{aligned}$$

and

$$C_2 F_\gamma = C_2 \text{T.V.}(\gamma^\delta(\cdot, 0)) \leq C_2 \text{T.V.}(\gamma_0) \leq \frac{C}{18}.$$

Hence, by Proposition 3.5,  $G$  decreases and

$$F_1(t_n) + \frac{1}{2}F_2(t_n) + kF_3(t_n) \leq \frac{4}{3}L(t_0).$$

We first find a bound on  $\text{T.V.}(u^\delta(\cdot, t_n))$ . If there were no non-physical fronts, we would have

$$\sum_{\text{rf}} \llbracket u \rrbracket = \sum_{\text{shock}} \llbracket u \rrbracket + u(\infty, \cdot) - u(-\infty, \cdot),$$

because  $u$  is increasing along all rarefaction waves and decreasing along all shock waves. Here  $\llbracket u \rrbracket := |u_r - u_l|$  for a wave connecting  $U_l$  to  $U_r$ , and rf is short for rarefaction wave. Let  $u_\pm = u_0(\pm\infty)$  and define

$$(3.33) \quad c_0 := |u(\infty, \cdot) - u(-\infty, \cdot)| = |u_+ - u_-|,$$

observing that  $u(\pm\infty, \cdot) = u_0(\pm\infty)$ . Taking the non-physical fronts into account, we have

$$\sum_{\text{rf}} \llbracket u \rrbracket \leq \sum_{\text{shock}} \llbracket u \rrbracket + \sum_{\text{np}} \llbracket u \rrbracket + c_0,$$

where np is short for non-physical front. Thus,

$$\begin{aligned} \text{T.V.}(u^\delta(\cdot, t_n)) &= \sum_{\text{rf}} \llbracket u \rrbracket + \sum_{\text{shock}} \llbracket u \rrbracket + \sum_{\text{np}} \llbracket u \rrbracket \leq 2 \sum_{\text{shock}} \llbracket u \rrbracket + 2 \sum_{\text{np}} \llbracket u \rrbracket + c_0 \\ &\leq 2s'_{\max} \sum_{\text{shock}} \llbracket p \rrbracket + 2F_3(t_n) + c_0 \leq 2s'_{\max}(F_1(t_n) + kF_3(t_n)) + c_0 \\ &\leq 2s'_{\max} \frac{4}{3}L(t_0) + c_0 \leq \left(\frac{8}{3}c_F + 1\right) \text{T.V.}(p_0, u_0) = \kappa \text{T.V.}(p_0, u_0), \end{aligned}$$

where we have used that  $c_0 \leq \text{T.V.}(u_0)$  and  $ks'_{\max} \geq 1$ . For  $\text{T.V.}(p^\delta(\cdot, t_n))$  we find

$$\begin{aligned} \text{T.V.}(p^\delta(\cdot, t_n)) &= \sum_{\text{rf}} \llbracket p \rrbracket + \sum_{\text{shock}} \llbracket p \rrbracket \leq k \left( \sum_{\text{rf}} \llbracket u \rrbracket + \sum_{\text{shock}} \llbracket u \rrbracket \right) \\ &\leq k \text{T.V.}(u^\delta(\cdot, t_n)) \leq \kappa k \text{T.V.}(p_0, u_0). \end{aligned}$$

Hence,

$$\begin{aligned} \text{T.V.}(p^\delta(\cdot, t_n), u^\delta(\cdot, t_n)) &= \text{T.V.}(p^\delta(\cdot, t_n)) + \text{T.V.}(u^\delta(\cdot, t_n)) \\ &\leq 2\kappa k \text{T.V.}(p_0, u_0). \end{aligned}$$

□

Next, we show that  $U^\delta \in \mathcal{U} \subset \mathcal{D}$  and determine  $p_{\max} \geq p_{\min} > 0$  and  $\bar{\gamma}$ . First of all,  $\gamma$  never takes any other values than those of the piecewise constant approximation of  $\gamma_0$ , thus,  $\bar{\gamma} = \sup_x \gamma_0(x)$ . From

$$\sup(y) \leq |y(\infty)| + |y(-\infty)| + \text{T.V.}(y),$$

and the fact that  $p^\delta(\pm\infty, \cdot) = p_0(\pm\infty) := p_\pm$ , it follows that

$$\begin{aligned} \sup(p^\delta - p_+) &\leq |p^\delta(\infty, \cdot) - p_+| + |p^\delta(-\infty, \cdot) - p_+| + \text{T.V.}(p^\delta) \\ &= |p_+ - p_-| + \text{T.V.}(p^\delta) \\ &\leq 2\text{T.V.}(p^\delta) \leq 2\kappa k \text{T.V.}(p_0, u_0). \end{aligned}$$

Similarly, we obtain

$$\begin{aligned}\sup(p^\delta - p_-) &\leq 2\kappa k T.V.(p_0, u_0), \\ \sup(u^\delta - u_+) &\leq 2\kappa T.V.(p_0, u_0), \\ \sup(u^\delta - u_-) &\leq 2\kappa T.V.(p_0, u_0).\end{aligned}$$

Hence, the approximate solution obtained by front tracking will always be contained in the domain

$$(3.34) \quad \mathcal{U} = \left\{ (p, u, \gamma) \mid \max\{|p - p_-|, |p - p_+|\} \leq 2\kappa k T.V.(p_0, u_0), \right. \\ \left. \max\{|u - u_-|, |u - u_+|\} \leq 2\kappa T.V.(p_0, u_0), \gamma \in (1, \bar{\gamma}] \right\},$$

where  $p_\pm = p_0(\pm\infty)$  and  $u_\pm = u_0(\pm\infty)$ . This means that we can determine  $p_{\max}$  and  $p_{\min}$  as follows: Choose  $p_{\max}$  as small as possible and  $p_{\min}$  as large as possible so that they satisfy

$$(3.35) \quad \begin{aligned}2\kappa(p_{\max}, p_{\min})k(p_{\max})T.V.(p_0, u_0) &\leq p_{\max} - \min\{p_-, p_+\}, \\ 2\kappa(p_{\max}, p_{\min})k(p_{\max})T.V.(p_0, u_0) &\leq \max\{p_-, p_+\} - p_{\min}.\end{aligned}$$

Despite the implicit equations,  $p_{\min}$  and  $p_{\max}$  only depend on the initial data. Thus, if the initial data are such that we from (3.35) find  $p_{\max} \geq p_0 \geq p_{\min} > 0$  and they satisfy condition (3.14), then  $U^\delta \in \mathcal{U}$  is bounded away from vacuum. In order to get (3.35), we have done several crude approximations, thus, initial data not satisfying (3.35) for a positive  $p_{\min}$  could still be initial data for which we never get vacuum. However, we cannot guarantee this a priori.

**3.6. Convergence to a weak solution.** The approximate solution,  $U^\delta$ , is bounded and, in particular, bounded away from vacuum. Furthermore, the total variation of  $U^\delta$  is bounded independent of  $\delta$ , as shown in the previous section. Since  $v = p^{-1/\gamma}$ , we furthermore have that  $v^\delta$  is bounded and have bounded total variation independent of  $\delta$ . Thus, the approximate solution given in the conservative variables,  $\tilde{U}^\delta = (v^\delta, u^\delta, \gamma^\delta)$ , is bounded, and

$$(3.36) \quad \text{T.V.}(\tilde{U}^\delta(\cdot, t)) \leq M_0,$$

for a constant  $M_0$  independent of  $\delta$ .

We first use Kolmogorov's compactness theorem [13, Thm. A.5] to show that there is a subsequence of  $\{\tilde{U}^\delta\}_{\delta>0}$  that converges in  $L^1_{\text{loc}}(\mathbb{R} \times [0, T])$ . To that end we observe that

$$(3.37) \quad \int_{\mathbb{R}} \left| \tilde{U}^\delta(x + \omega, t) - \tilde{U}^\delta(x, t) \right| dx \leq \omega \text{T.V.}(\tilde{U}^\delta(\cdot, t)) \leq M_0 \omega.$$

Thus, it remains to show that for any  $R > 0$ ,

$$(3.38) \quad \int_{-R}^R \left| \tilde{U}^\delta(x, t) - \tilde{U}^\delta(x, s) \right| dx \leq M_1(t - s),$$

where  $t \geq s \geq 0$  and  $M_1$  is independent of  $\delta$ . See Theorem A.8 in [13] for a detailed proof of why (3.36)-(3.38) yield a convergent subsequence using Kolmogorov's compactness theorem. Here we proceed by showing that (3.38) holds for our system.

For  $t \in (\tau_i, \tau_{i+1}]$ , where  $\tau_i$  and  $\tau_{i+1}$  are two consecutive collision times, we can write  $\tilde{U}^\delta$  as

$$\tilde{U}^\delta(x, t) = \sum_{k=1}^{N_{\tau_i}} (U_{k-1}^i - U_k^i) H(x - x_k^i(t)) + U_{N_{\tau_i}},$$

where  $x_k^i$  is the position of the  $k$ th front from the left,  $H$  is the Heaviside function,  $N_{\tau_i}$  is the number of fronts after the collision at  $\tau_i$ , and  $\tilde{U}^\delta(x, t) = U_k^i$  for  $x \in$

$(x_k^i, x_{k+1}^i)$ . Assume now that  $t \in (\tau_i, \tau_{i+1}]$  and  $s \in (\tau_j, \tau_{j+1}]$  where  $j \leq i$  and  $s \leq t$ . Then

$$\begin{aligned} \int_{\mathbb{R}} \left| \tilde{U}^\delta(x, t) - \tilde{U}^\delta(x, \tau_i) \right| dx &= \int_{\mathbb{R}} \left| \int_{\tau_i}^t \frac{d}{dt} \tilde{U}^\delta(x, \hat{t}) d\hat{t} \right| dx \\ &\leq \int_{\mathbb{R}} \int_{\tau_i}^t \sum_{k=1}^{N_{\tau_i}} |U_{k-1}^i - U_k^i| \left| \frac{d}{dt} x_k^i(\hat{t}) \right| |H'(x - x_k^i(\hat{t}))| d\hat{t} dx \\ &\leq \lambda_{\text{np}} \int_{\tau_i}^t \sum_{k=1}^{N_{\tau_i}} |U_{k-1}^i - U_k^i| \int_{\mathbb{R}} |H'(x - x_k^i(\hat{t}))| dx d\hat{t} \\ &\leq \lambda_{\text{np}}(t - \tau_i) \text{T.V.}(\tilde{U}^\delta(\cdot, t)) \leq \lambda_{\text{np}} M_0(t - \tau_i), \end{aligned}$$

where we have used that  $\left| \frac{d}{dt} x_k^i(\hat{t}) \right| \leq \lambda_{\text{np}}$ . By similar arguments we get

$$\begin{aligned} \int_{\mathbb{R}} \left| \tilde{U}^\delta(x, \tau_i) - \tilde{U}^\delta(x, \tau_{j+1}) \right| dx &\leq \lambda_{\text{np}} M_0(\tau_i - \tau_{j+1}), \quad \text{if } j+1 < i, \\ \int_{\mathbb{R}} \left| \tilde{U}^\delta(x, \tau_{j+1}) - \tilde{U}^\delta(x, s) \right| dx &\leq \lambda_{\text{np}} M_0(\tau_{j+1} - s). \end{aligned}$$

Hence,

$$\begin{aligned} \int_{\mathbb{R}} \left| \tilde{U}^\delta(x, t) - \tilde{U}^\delta(x, s) \right| dx &\leq \int_{\mathbb{R}} \left| \tilde{U}^\delta(x, t) - \tilde{U}^\delta(x, \tau_i) \right| dx \\ &\quad + \int_{\mathbb{R}} \left| \tilde{U}^\delta(x, \tau_i) - \tilde{U}^\delta(x, \tau_{j+1}) \right| dx + \int_{\mathbb{R}} \left| \tilde{U}^\delta(x, \tau_{j+1}) - \tilde{U}^\delta(x, s) \right| dx \\ &\leq \lambda_{\text{np}} M_0(t - s), \end{aligned}$$

where the middle integral is only included if  $j+1 < i$ . Since  $\lambda_{\text{np}} M_0$  is a constant independent of  $\delta$ , we have now established (3.38). Hence, there exists a function  $U(x, t)$  and a subsequence  $\{\delta_j\} \subset \{\delta\}$  so that  $\tilde{U}^{\delta_j} \rightarrow U$  in  $L^1_{\text{loc}}(\mathbb{R} \times [0, T])$  as  $j \rightarrow \infty$ .

We still have to show that the limit is a weak solution. Recall from equation (2.1) that  $U = (v, u, \gamma)$  is a weak solution on a strip  $[t, s]$  if

$$\begin{aligned} \mathcal{I}_t^s(U) &:= \int_t^s \int_{\mathbb{R}} U \phi_t + f(U) \phi_x dx dt \\ &\quad - \int_{\mathbb{R}} U(x, s) \phi(x, s) dx + \int_{\mathbb{R}} U(x, t) \phi(x, t) dx = 0, \end{aligned}$$

for all test functions  $\phi$ . Fix two successive collision times,  $\tau_j$  and  $\tau_{j+1}$ , and let  $\tilde{U}^\delta$  be the approximate solution found using front tracking. The approximate solution  $\tilde{U}^\delta$  is not a weak solution because we have introduced non-physical fronts, changed the speed of some fronts, and approximate rarefaction waves. Therefore, we need to estimate how far  $\tilde{U}^\delta$  is from the weak solution.

Let  $s_1 = \tau_j$  and let  $V_i(x, s)$  be the weak solution of

$$(3.39) \quad V_t + f(V)_x = 0, \quad V(x, s_i) = \tilde{U}^\delta(x, s_i).$$

We find  $V_1$  for  $t$  close to  $s_1$  by solving exactly the Riemann problems at the jumps of  $\tilde{U}^\delta(x, s_1)$ . This solution is defined up to the time  $s_2 > s_1$  when the first waves interact. If no waves in  $V_1$  collide before  $\tau_{j+1}$ , we have  $s_2 = \tau_{j+1}$ . Otherwise, we let  $V_2$  be the solution of (3.39) for  $s \geq s_2$  with  $i = 2$  and  $\tilde{U}^\delta(x, s_2)$  as initial data. In this way we fill  $[\tau_j, \tau_{j+1})$  with small strips  $[s_i, s_{i+1})$  on which we have defined  $V_i$ . On each strip we also define  $V_i^\delta$  as the approximated solution of (3.39) where the approximated Riemann solver is used. Thus,  $V_i^\delta$  has no non-physical fronts and none of its fronts interact before  $t = s_{i+1}$ , so none of the fronts have altered speeds.

Let us now define  $V$  and  $V^\delta$  on  $[\tau_j, \tau_{j+1})$  as the functions that equals  $V_i$  and  $V_i^\delta$ , respectively, at each interval  $[s_i, s_{i+1})$ . Thus,  $V$  is the exact solution on each strip and  $V^\delta$  only differs from  $V$  for the approximated rarefaction waves. Note that  $V^\delta(x, s_i) = V(x, s_i) = \tilde{U}^\delta(x, s_i)$  for each  $i$ .

Figure 14(a) shows this construction when a non-physical front is present in  $\tilde{U}^\delta$ , Figure 14(b) shows the first steps in the construction when a rarefaction front interacts with a front of the same family at  $\tau_{j+1}$  and Figure 14(c) illustrates the case where there is a front with shifted speed in  $\tilde{U}^\delta$ .

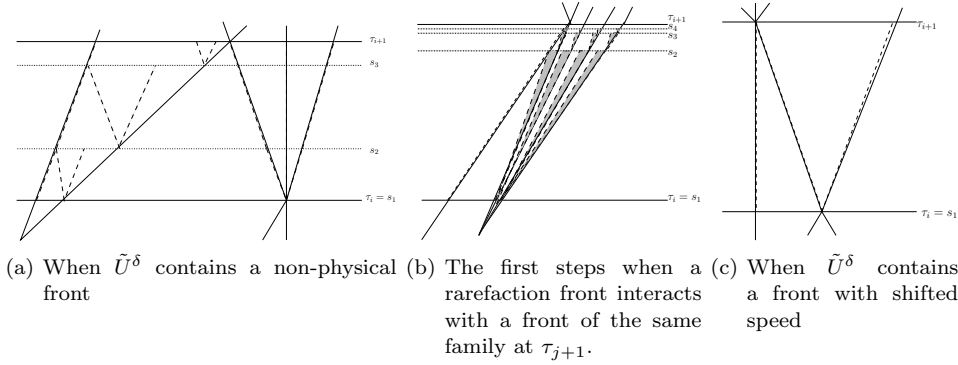


FIGURE 14. The approximate solution  $\tilde{U}^\delta$  (solid lines) and the exact solution  $V_i$  (dashed line) at each interval  $[s_i, s_{i+1})$ .

Let us first estimate the difference between  $V^\delta$  and  $V$ , that is, the error we do when approximating the rarefaction fan as rarefaction fronts. This is done so that  $|V_i^\delta(x, t) - V_i(x, t)| = \mathcal{O}(\delta)$  for  $(x, t)$  in a rarefaction fan. Thus, for  $t \in [s_i, s_{i+1})$ , the integral

$$\int_{\mathbb{R}} |V^\delta(x, t) - V(x, t)| dx,$$

will be the sum of the integrals across the rarefaction fans of  $V$ . Let  $V_l$  and  $V_r$  be the left and right state of such a fan. The integral over this fan will be the sum of the integrals across each step in  $V^\delta$ , and there are  $|p_r - p_l|/\mathcal{O}(\delta)$  steps, each with the width  $(t - s_i)\Delta\lambda = (t - s_i)\mathcal{O}(\delta)$ , where  $\Delta\lambda$  is the difference in the characteristic speed across a rarefaction-front in  $V^\delta$ . We sum over  $j$ , that is, over all rarefaction fans in  $V$ , and find that

$$(3.40) \quad \int_{\mathbb{R}} |V^\delta(x, t) - V(x, t)| dx = \sum_j \frac{|p_r^j - p_l^j|}{\mathcal{O}(\delta)} \mathcal{O}(\delta)(t - s_i)\mathcal{O}(\delta) \leq (t - s_i)\text{T.V.}(p^\delta)\mathcal{O}(\delta) \leq (t - s_i)\mathcal{O}(\delta),$$

since  $\sum_j |p_r^j - p_l^j| \leq \text{T.V.}(p^\delta) \leq M_0$ .

Next, we compare  $V^\delta$  to  $U^\delta$ . Since  $U^\delta(x, s_i)$  is used as initial data solving (3.39) for each strip, the two solutions only differs where  $U^\delta$  have Riemann problems solved by the simplified solver or where the speed of a front in  $U^\delta$  has been shifted. Thus, in order to estimate the integral

$$(3.41) \quad \int_{\mathbb{R}} |U^\delta(x, t) - V^\delta(x, t)| dx,$$

for a  $t \in [s_i, s_{i+1})$ , we first take a closer look at the approximation done using the simplified Riemann solver defined in Section 3.1. Consider the interaction  $\zeta + \epsilon$

and note that the arguments are similar for the symmetric interaction. As in Lemma 3.3, we let  $\hat{\epsilon} + \zeta + \hat{\eta}$  with intermediate states  $\hat{U}_i$ ,  $i = 1, 2$ , be the solution using the approximate solver, and  $\epsilon' + \zeta + \theta^{\text{np}}$  with intermediate states  $\tilde{U}_i$ ,  $i = 1, 2$  be the solution using the simplified solver. If  $\epsilon'$  is a shock-front, then  $\alpha'$  and  $\hat{\alpha}$  have slightly different speeds giving rise to a jump in  $|U^\delta - V^\delta|$  of the width  $|\sigma_{\hat{\alpha}} - \sigma_{\alpha'}|(t - s_i) = \mathcal{O}(1)|\theta^{\text{np}}|(t - s_i)$ , cf. Lemma 3.3. If  $\epsilon'$  is a rarefaction-front, the speeds are equal. Furthermore,  $|U^\delta - V^\delta|$  has the jumps  $|\hat{U}_1 - \tilde{U}_1|$ ,  $|\hat{U}_2 - \tilde{U}_2|$ , and  $|U_r - \tilde{U}_2|$ . From Lemma 3.3 we have that the heights of these jumps are all bounded by  $\mathcal{O}(1)|\theta^{\text{np}}|$ . Next, we look at the case where  $U^\delta$  has a front whose speed is changed by  $\delta_\sigma$  and we denote it by  $\theta_{\delta_\sigma}$ . Then we have an interval of length  $\delta_\sigma(t - s_i)$  where  $|U^\delta - V_i^\delta| = |\theta_{\delta_\sigma}|$ . Thus,

$$\begin{aligned}
(3.42) \quad & \int_{\mathbb{R}} |U^\delta(x, t) - V^\delta(x, t)| dx \\
& \leq \sum_{\theta^{\text{np}} \text{ in } U^\delta} \mathcal{O}(1)|\theta^{\text{np}}|(t - s_i) + \sum_{\theta_{\delta_\sigma} \text{ in } U^\delta} |\theta_{\delta_\sigma}| \delta_\sigma(t - s_i) \\
& = (\mathcal{O}(1)\delta_{\text{init}} + \delta_\sigma \text{T.V.} U^\delta(x, t))(t - s_i) = \mathcal{O}(1)\delta(t - s_i),
\end{aligned}$$

where we have used that  $\sum |\theta^{\text{np}}| \leq \mathcal{O}(1)\delta_{\text{init}} = \mathcal{O}(1)\delta$  according to Lemma 3.12, and that  $\sum_{\theta_{\delta_\sigma} \text{ in } U^\delta} |\theta_{\delta_\sigma}| \leq \text{T.V.} U^\delta(x, t) \leq M_0$  and  $\delta_\sigma = \mathcal{O}(1)\delta$ .

Combining (3.40) and (3.42), we finally get

$$\begin{aligned}
\int_{\mathbb{R}} |U^\delta(x, t) - V(x, t)| dx & \leq \int_{\mathbb{R}} |U^\delta(x, t) - V^\delta(x, t)| + \int_{\mathbb{R}} |V^\delta(x, t) - V(x, t)| \\
& = \mathcal{O}(\delta)(t - s_i).
\end{aligned}$$

Our goal is to show that  $|\mathcal{I}_0^T(U)| = 0$  where  $U(x, t)$  is the limit of  $\tilde{U}^{\delta_j}(x, t)$ . We start by estimating  $|\mathcal{I}_{s_i}^{s_{i+1}}(\tilde{U}^\delta)|$ . Recall that  $V_i(x, s_i) = \tilde{U}^\delta(x, s_i)$  and that  $V_i$  is a weak solution on each strip, thus,  $\mathcal{I}_{s_i}^{s_{i+1}}(V_i) = 0$ . We start with  $v^\delta$ ;

$$\begin{aligned}
|\mathcal{I}_{s_i}^{s_{i+1}}(v^\delta)| & = |\mathcal{I}_{s_i}^{s_{i+1}}(v^\delta) - \mathcal{I}_{s_i}^{s_{i+1}}(v_i)| \\
& = \left| \int_{s_i}^{s_{i+1}} \int_{\mathbb{R}} (v^\delta - v_i) \phi_t + (-u^\delta + u_i) \phi_x dx dt \right. \\
& \quad \left. - \int_{\mathbb{R}} (v^\delta(x, s_{i+1}) - v_i(x, s_{i+1})) \phi(x, s_{i+1}) dx \right| \\
& \leq M_2 \left( \int_{s_i}^{s_{i+1}} \int_{\mathbb{R}} |v^\delta - v_i| + |u^\delta - u_i| dx dt \right. \\
& \quad \left. + \int_{\mathbb{R}} |v^\delta(x, s_{i+1}) - v_i(x, s_{i+1})| dx \right) \\
& \leq \mathcal{O}(\delta) ((s_{i+1} - s_i)^2 + (s_{i+1} - s_i)),
\end{aligned}$$

where  $M_2$  bounds  $|\phi_x|$  and  $|\phi_t|$ . For  $u^\delta$  we get

$$\begin{aligned} |\mathcal{I}_{s_i}^{s_{i+1}}(u^\delta)| &= |\mathcal{I}_{s_i}^{s_{i+1}}(u^\delta) - \mathcal{I}_{s_i}^{s_{i+1}}(u_i)| \\ &= \left| \int_{s_i}^{s_{i+1}} \int_{\mathbb{R}} (u^\delta - u_i) \phi_t + (p^\delta - p_i) \phi_x dx dt \right. \\ &\quad \left. - \int_{\mathbb{R}} (u^\delta(x, s_{i+1}) - u_i(x, s_{i+1})) \phi(x, s_{i+1}) dx \right| \\ &\leq M_2 \left( \int_{s_i}^{s_{i+1}} \int_{\mathbb{R}} |u^\delta - u_i| + |p^\delta - p_i| dx dt \right. \\ &\quad \left. + \int_{\mathbb{R}} |u^\delta(x, s_{i+1}) - u_i(x, s_{i+1})| dx \right) \\ &\leq \mathcal{O}(\delta) ((s_{i+1} - s_i)^2 + (s_{i+1} - s_i)), \end{aligned}$$

where we have used that

$$\int_{\mathbb{R}} |p_i(x, t) - p^\delta(x, t)| dx \leq (t - s_i) \mathcal{O}(\delta),$$

by the same arguments as above. Since  $\gamma$  only changes along contact discontinuities and these are solved exactly both by the approximate and the simplified solver, and their speeds are never changed, we actually have  $\gamma_i(x, t) = \gamma^\delta(x, t)$ , thus

$$|\mathcal{I}_{s_i}^{s_{i+1}}(\gamma^\delta)| = |\mathcal{I}_{s_i}^{s_{i+1}}(\gamma_i)| = 0.$$

Let  $\tau_j$  and  $\tau_{j+1}$  still be two successive collision times and recall that  $\tau_{j+1} - \tau_j = \sum_{i=1}^{\infty} (s_{i+1} - s_i)$ . Thus,

$$\begin{aligned} |\mathcal{I}_{\tau_j}^{\tau_{j+1}}(\tilde{U}^\delta)| &\leq \sum_{i=1}^{\infty} |\mathcal{I}_{s_i}^{s_{i+1}}(\tilde{U}^\delta)| \\ &\leq \sum_{i=1}^{\infty} \mathcal{O}(\delta) ((s_{i+1} - s_i)^2 + (s_{i+1} - s_i)) \\ &\leq \mathcal{O}(\delta) ((\tau_{j+1} - \tau_j)^2 + (\tau_{j+1} - \tau_j)). \end{aligned}$$

Since  $\tilde{U}^\delta$  is bounded and  $\tilde{U}^{\delta_j}(x, t) \rightarrow U(x, t)$  in  $L_{\text{loc}}^1$  where  $U = (v, u, \gamma)$ ,  $p^\delta$  will converge to  $p = v^{-1/\gamma}$  in  $L_{\text{loc}}^1$ . Thus, for any time  $T < \infty$ ,

$$\begin{aligned} |\mathcal{I}_0^T(U)| &= \lim_{\delta \rightarrow 0} |\mathcal{I}_0^T(\tilde{U}^\delta)| = \lim_{\delta \rightarrow 0} \sum_j |\mathcal{I}_{\tau_j}^{\tau_{j+1}}(\tilde{U}^\delta)| \\ &= \lim_{\delta \rightarrow 0} \sum_j \mathcal{O}(\delta) ((\tau_{j+1} - \tau_j)^2 + (\tau_{j+1} - \tau_j)) \\ &\leq \lim_{\delta \rightarrow 0} \mathcal{O}(\delta)(T + T^2) = 0, \end{aligned}$$

which proves that  $\tilde{U}^\delta$  converges to a weak solution of (1.1) as  $\delta \rightarrow 0$ .

Thus, we have finally proved the main theorem:

**Theorem 3.14.** *Consider the Cauchy problem for system (1.1) with initial data (1.2) where  $\inf(p_0(x)) > 0$  and  $1 < \gamma_0(x) \leq \bar{\gamma}$  and  $p_{\max} \geq p_{\min} > 0$  can be determined from (3.35). Assume that the initial data  $(u_0(x), p_0(x))$  and  $\gamma_0(x)$  satisfy*

$$(3.43) \quad (\bar{\gamma} - 1) \text{T.V.}(p_0(x), u_0(x)) \leq \frac{C}{18kC_1},$$

$$(3.44) \quad \text{T.V.}(\gamma_0(x)) \leq \frac{C}{18C_2}.$$

*Then the front tracking algorithm produces a sequence of approximate solutions which converges to a global weak solution of the system (1.1).*

Note that all constants only depend on  $p_{\min}$ ,  $p_{\max}$  and  $\bar{\gamma}$ . Thus, by reducing  $\bar{\gamma}$ , we may allow arbitrary large total variation for  $p_0$  and  $u_0$ .

By the results of Wagner [25], there is a one-to-one correspondence between a weak solution of (1.1) and a weak solution of the system given in Eulerian coordinates,

$$(3.45) \quad \begin{aligned} \rho_t + (\rho u)_x &= 0, \\ (\rho u)_t + (\rho u^2 + p(\rho, \gamma))_x &= 0, \\ (\rho \gamma)_t + (\rho u \gamma)_x &= 0, \end{aligned}$$

where  $x \in \mathbb{R}$  is the physical space variable and  $t \in (0, \infty)$  denotes time.

#### 4. NUMERICAL EXAMPLES

In order to test the algorithm in practice we have used the front-tracking code from the web page of [13]<sup>1</sup>, supplemented by Riemann solvers specific to (1.1). The threshold parameter  $\rho$ , which determines when to invoke the simplified Riemann solver, is set to  $\delta^3$  for all examples. Furthermore, we let  $\lambda_{\text{np}} = 2\lceil \lambda_{\max} \rceil$ . The front-tracking code is slightly adjusted so that  $G(t)$  is computed for all times.

**Example 4.1.** The initial data in this example are piecewise constant and symmetric. We have one gas with  $p = 4.56$ ,  $u = 3.025$  and  $\gamma = 1.03$  which initially is trapped by another gas with  $p = 4.57$ ,  $u = 3.010$  and  $\gamma = 1.03$ . For this example

$p_{\max}$	$p_{\min}$	$\bar{\gamma}$	$C_1$	$C_2$	$C$	$k$
3.602	5.538	1.03	8.3743	5.5000	1	5.5000

TABLE 2. The constants for Example 4.1.

we have found  $p_{\min}$  and  $p_{\max}$  from (3.35). These and the other constants calculated for this example are listed in Table 2, and (3.30) is satisfied since

$$(4.1) \quad \begin{aligned} \text{T.V.}(p_0, u_0) &= 0.05 \leq 0.0804 = C/(18kC_1(\bar{\gamma} - 1)), \\ \text{T.V.}(\gamma_0) &= 0.02 \leq 0.0202 = C/(18C_2). \end{aligned}$$

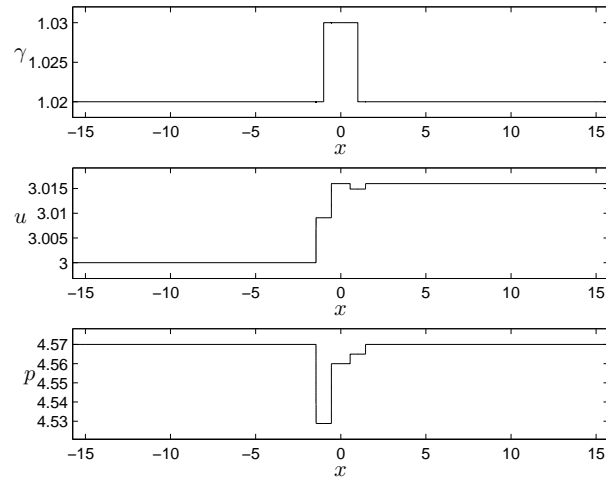
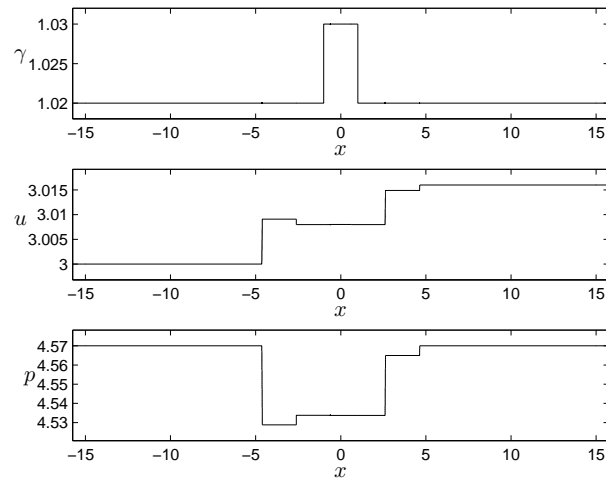
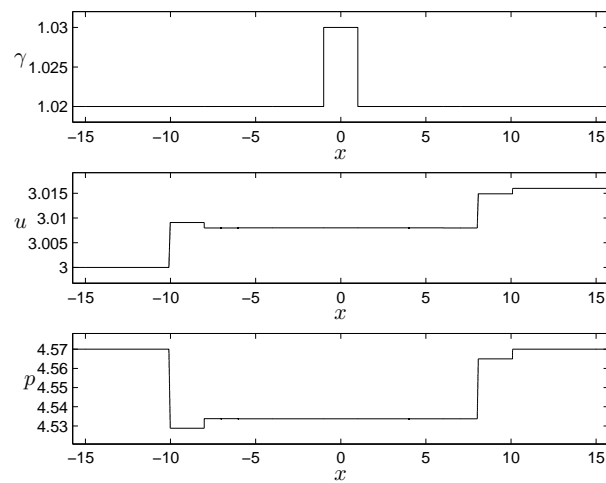
Figure 15 shows  $U^\delta(\cdot, t)$  at some different times. The front-tracking solution in the  $(x, t)$ -plane is shown in Figure 16. Here  $\delta = 0.001$ , thus, the rarefaction fronts are very close and look like rarefaction fans. Note furthermore that one front is one line regardless of its strength, thus, in Figure 16 one does not distinguish between strong and weak shock-fronts. In this example we see that after some time, several non-physical fronts are generated, and from then on, there is no more interactions with a contact discontinuity. Finally, Figure 19(a) shows  $G(t)$  for this example.

**Example 4.2.** The initial data in this example are also piecewise constant. For  $-1 < x < 1$  we have  $p = 3$  and  $u = 2.5$ , while we outside the unit interval have  $p = 1.5$  and  $u = 2.0$ . Furthermore,  $\gamma = 1.5$  for  $x < -1$  and  $0 < x < 1$  while  $\gamma = 2.0$  for  $-1 < x < 0$  and  $x > 1$ .

These initial data do not satisfy condition (3.30), and are therefore not covered by Theorem 3.14. Furthermore, we observe that  $p^\delta(x, t)$  always stays between 1.5 and 3.0 in this example, and therefore  $p_{\min} = 2.99$  and  $p_{\max} = 3.01$  are used to calculate the different constants. As shown in Figure 19(b), we still have that  $G(t)$  decreases for this example.

In Figure 17 we see  $U^\delta(\cdot, t)$  at some different times, while Figure 18 shows the solution in the  $(x, t)$ -plane. The split rarefaction waves are more visible here,

<sup>1</sup><http://www.math.ntnu.no/~holden/FrontBook/matlabcode.html>

(a)  $t = 0.1$ .(b)  $t = 0.8$ .(c)  $t = 2.0$ .FIGURE 15. The solution  $U^\delta(\cdot, t)$  at different times  $t$  for Example 4.1.

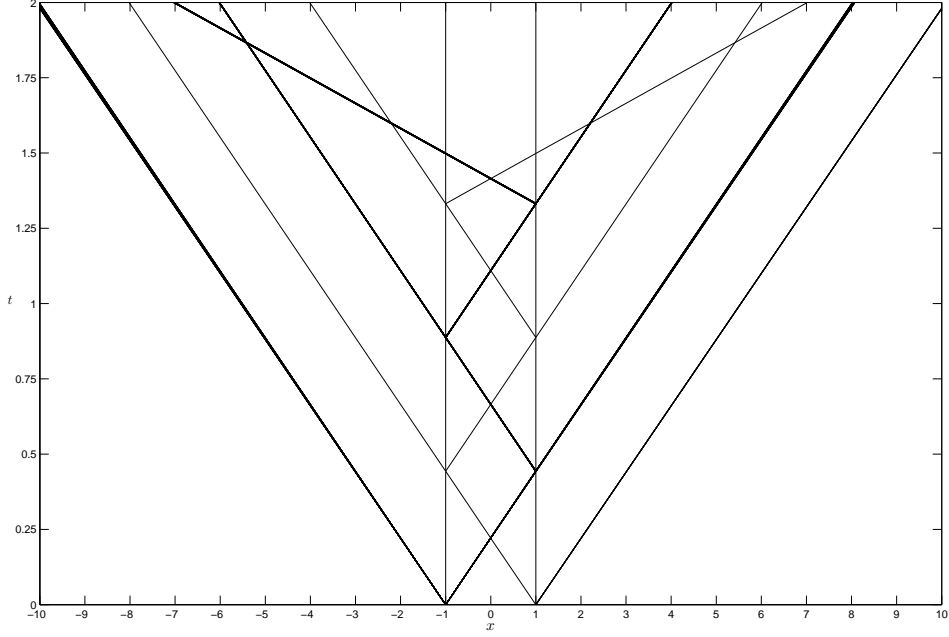


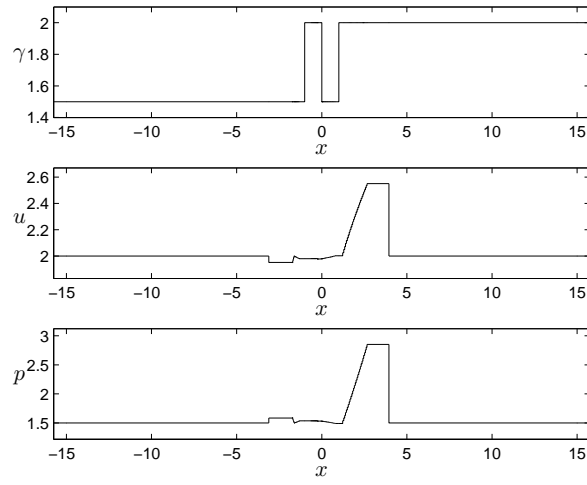
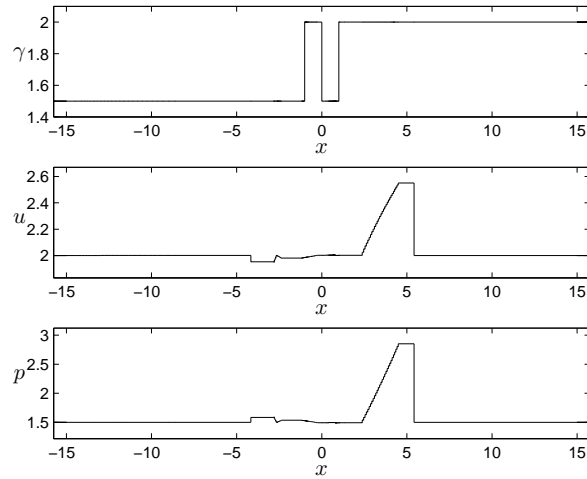
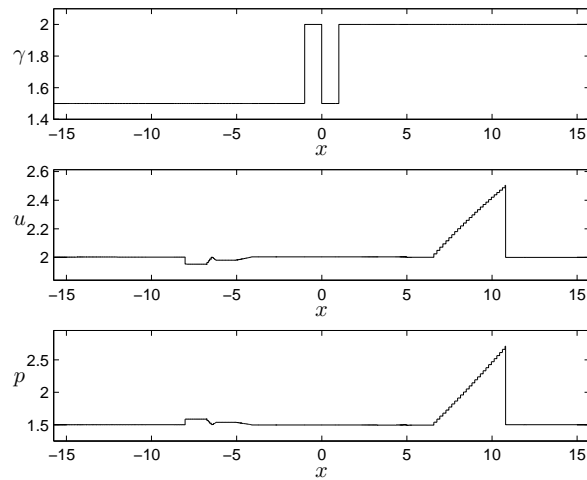
FIGURE 16. The solution  $U^\delta(x, t)$  in the  $(x, t)$ -plane for Example 4.1.

were we have used  $\delta = 0.05$ . Initially we have three Riemann problems. The solution of the one situated at  $x = -1$  is a 1-shock wave, a contact discontinuity and a 3-rarefaction wave, the one situated at  $x = 1$  is almost symmetric with a solution consisting of a small 1-rarefaction wave, a contact discontinuity and a 3-shock wave, while at  $x = 0$  we have only a jump in  $\gamma$ , hence, the solution is a single contact discontinuity. We see that the first non-physical fronts are generated when reflected fronts of a  $\gamma$ -collision interacts with another contact discontinuity. The reflected fronts become weaker for each  $\gamma$ -collision, thus, after some time, all fronts present between the contact discontinuities are non-physical fronts. These non-physical fronts just pass through the contact discontinuities without generating more reflected fronts. Recall that  $p$  and  $\gamma$  are constant across non-physical fronts, thus, comparing the plots for  $p$  and  $u$  in Figure 17 we see that the non-physical fronts are small compared to the physical fronts.

**Example 4.3.** In this example  $\gamma_0$  is a continuous function where  $\gamma_0 = 2.7406$  for  $x \leq -0.5$ ,  $\gamma_0 = 3.6994$  for  $x \geq 0.4$  and increases smoothly from 2.7406 to 3.6994 by a sine function in the region  $-0.5 \leq x \leq 0.4$ . In the same region we have a high initial pressure,  $p_0 = 8$ , while  $p_0 = 3$  outside. The velocity is piecewise constant and decaying;  $u_0 = 3$  for  $x \leq -0.5$ ,  $u_0 = 2$  for  $-0.5 \leq x \leq 0.4$  and  $u_0 = 1$  for  $x \geq 0.4$ . The initial data are made piecewise constant with  $\delta_{\text{init}} = \Delta x = 0.1$ , giving rise to several contact discontinuities separated by  $\Delta x$ . Furthermore, we have chosen  $\delta = 0.2$ .

These initial data are far from satisfying condition (3.30), but  $G$  is still decreasing as shown in in Figure 19(c). For this example we have found that  $2.8 < p^\delta(x, t) < 17.5$ , and these values are selected for  $p_{\min}$  and  $p_{\max}$  and used in the calculations.

In Figure 20 we see  $U^\delta(\cdot, t)$  at some different times, while Figure 21 shows the solution in the  $(x, t)$ -plane. In Figure 21 we observe a lot of fronts interacting, but Figure 20 reveals that after a short time, all fronts except the leftmost and rightmost shocks are very weak fronts, including the non-physical fronts. This is

(a)  $t = 1.2$ .(b)  $t = 1.8$ .(c)  $t = 4.0$ .FIGURE 17.  $U^\delta(\cdot, t)$  at different times  $t$  for Example 4.2.

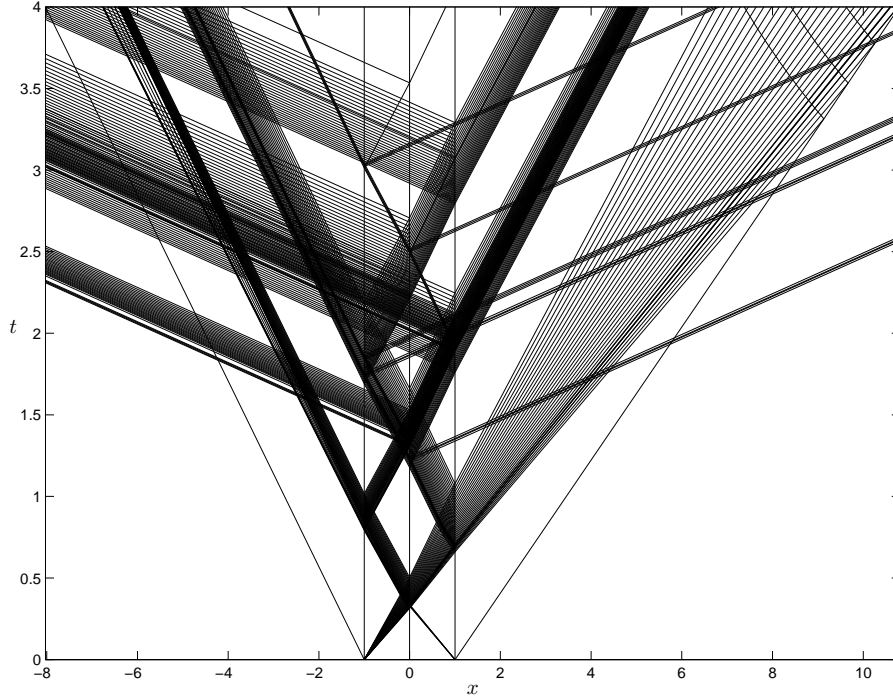


FIGURE 18. The solution  $U^\delta(x, t)$  in the  $(x, t)$ -plane for Example 4.2.

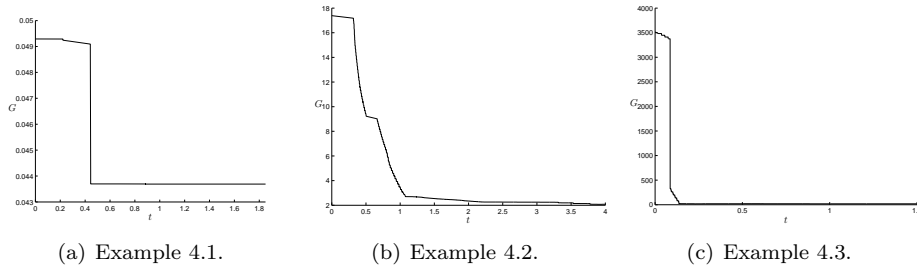


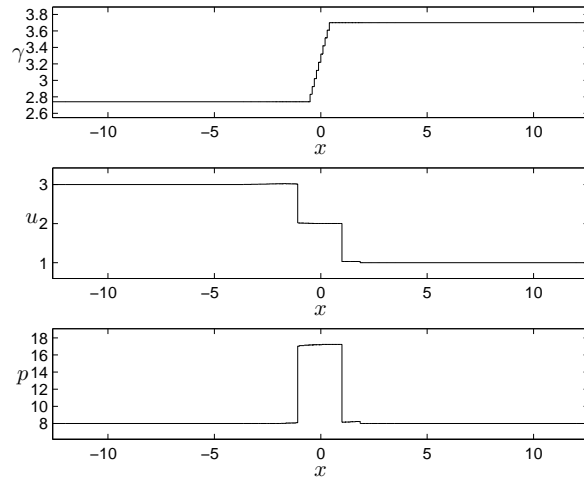
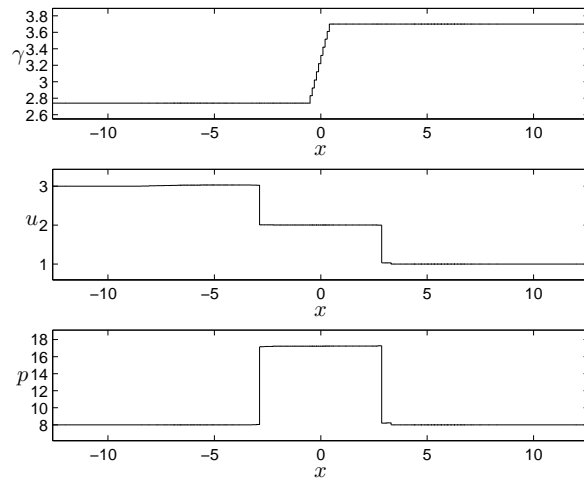
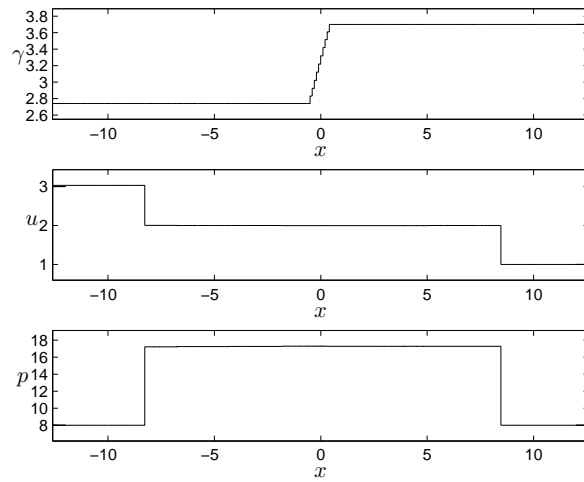
FIGURE 19.  $G$  for the three examples.

also in accordance with Figure 19(c) where we after a short time have only very small changes in  $G$ .

**Acknowledgment.** We are exceptionally grateful to Debora Amadori and Hermano Frid for extensive discussions and help on this model.

#### REFERENCES

- [1] D. Amadori and A. Corli. On a model of multiphase flow. *SIAM J. Math. Anal.*, 40(1):134–166, 2008.
- [2] F. Asakura. Wave-front tracking for the equation of non-isentropic gas dynamics. *RIMS Kokyuroku*, 1495:78–91, 2006.
- [3] F. Asakura. Wave-front tracking for the equation of isentropic gas dynamics. *Quart. Appl. Math.*, 63(1):20–33, 2005.
- [4] A. Bressan. *Hyperbolic Systems of Conservation Laws*. Oxford University Press, 2000.
- [5] A. Bressan and R. M. Colombo. Unique solutions of  $2 \times 2$  conservation laws with large data. *Indiana Univ. Math. J.*, 44(3):677–725, 1993.

(a)  $t = 0.1$ .(b)  $t = 0.4$ .(c)  $t = 1.0$ .FIGURE 20.  $U^\delta(\cdot, t)$  at different times  $t$  for Example 4.3.

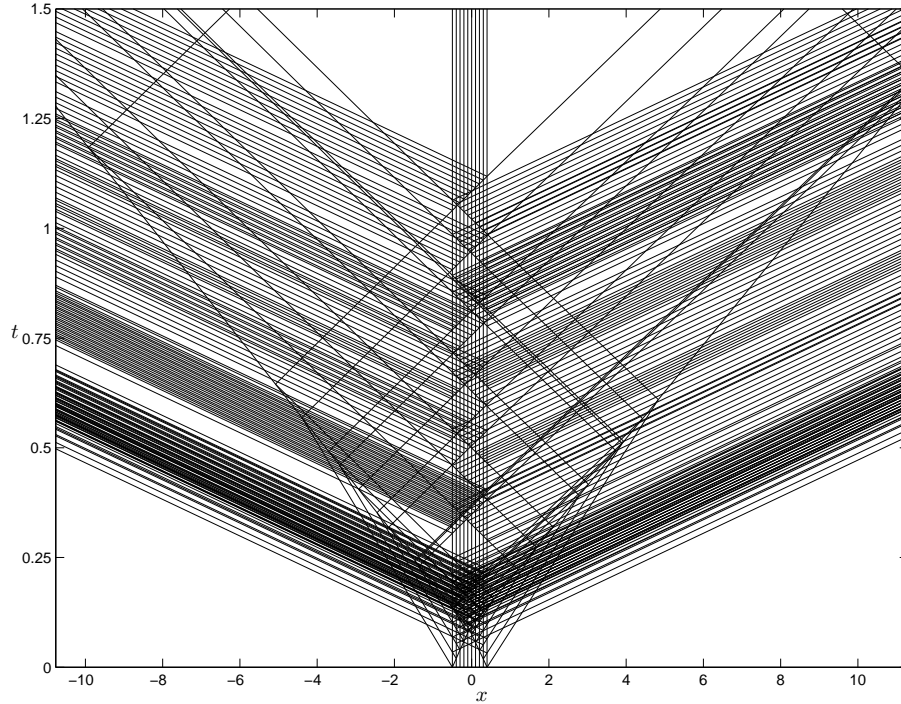


FIGURE 21. The solution  $U^\delta(x, t)$  in the  $(x, t)$ -plane for Example 4.3.

- [6] C. Chalons and F. Coquel. Navier–Stokes equations with several independent pressure laws and explicit predictor-corrector schemes. *Numer. Math.* 101:451–478, 2005.
- [7] G.-Q. Chen, C. Christoforou, and Y. Zhang. Dependence of entropy solutions in the large for the Euler equations on nonlinear flux functions. *Indiana Univ. Math. J.* 56(5):2535–2567, 2007.
- [8] G.-Q. Chen, C. Christoforou, and Y. Zhang. Continuous dependence of entropy solutions to the Euler equations on the adiabatic exponent and Mach number. *Arch. Ration. Mech. Anal.* 189:97–130, 2008.
- [9] R. J. DiPerna. Existence in the large for quasilinear hyperbolic conservation laws. *Arch. Rational Mech. Anal.*, 52:244–257, 1973.
- [10] S. Evje and K. H. Karlsen. Global existence of weak solutions for a viscous two-phase model. *J. Differential Equations*, 245(9):2660–2703, 2008.
- [11] H. Fan. On a model of the dynamics of liquid/vapor phase transitions. *SIAM J. Appl. Math.*, 60(4):1270–1301. 2000.
- [12] J. Glimm. Solution in the large for nonlinear hyperbolic systems of equations. *Comm. Pure Appl. Math.*, 18:697–715, 1965.
- [13] H. Holden and N. H. Risebro. *Front Tracking for Hyperbolic Conservation Laws*. Springer-Verlag, revised printing, 2007.
- [14] H. Holden, N. H. Risebro and H. Sande. The solution of the Cauchy problem with large data for a model of a mixture of gases. *J. Hyperbolic Differ. Eq.*, 6(1):25–106, 2009.
- [15] T.-P. Liu. Solutions in the large for the equations of nonisentropic gas dynamics. *Indiana Univ. Math. J.*, 26(1):147–177, 1977.
- [16] T. P. Liu and J. A. Smoller. On the vacuum state for the isentropic gas dynamics equations. *Adv. in Appl. Math.*, 1(4):345–359, 1980.
- [17] Y. Lu. *Hyperbolic Conservation Laws and the Compensated Compactness Method*. Shapman&Hall/CRC, 2003.
- [18] T. Nishida. Global solution for an initial boundary value problem for a quasilinear hyperbolic system. *Proc. Japan Acad.*, 44:642–646, 1968.
- [19] T. Nishida and J. A. Smoller. Solution in the large for some nonlinear hyperbolic conservation laws. *Comm. Pure Appl. Math.*, 26:183–200, 1973.

- [20] Y.-J. Peng. Solutions faibles globales pour l'équation d'Euler d'un fluide compressible avec de grandes données initiales. *Comm. Partial Differential Equations*, 17(1-2):161–187, 1992.
- [21] Y.-J. Peng. Solutions faibles globales pour un modèle d'écoulements diphasiques. *Ann. Scuola Norm. Sup. Pisa Cl. Sci. (4)*, 21(4):523–540, 1994.
- [22] J. Smoller. *Shock Waves and Reaction-Diffusion Equations*. Springer-Verlag, second edition, 1994.
- [23] J. B. Temple. Solution in the large for the nonlinear hyperbolic conservation laws of gas dynamics. *J. Differential Equations*, 41:96–161, 1981.
- [24] B. Temple and R. Young. The large time stability of sound waves. *Comm. Math. Phys.*, 179(2):417–466, 1996.
- [25] D. H. Wagner. Equivalence of the Euler and Lagrangian equations of gas dynamics for weak solutions. *J. Differential Equations*, 68(1):118–136, 1987.
- [26] W.-A. Yong. A simple approach to Glimm's interaction estimates. *Appl. Math. Lett.*, 12(2):29–34, 1999.
- [27] B. D. Wissman. Global solutions to the ultra-relativistic Euler equations. arXiv:0705.1333v1 [math.AP] 9 May 2007.

(Holden)

DEPARTMENT OF MATHEMATICAL SCIENCES, NORWEGIAN UNIVERSITY OF SCIENCE AND TECHNOLOGY, NO-7491 TRONDHEIM, NORWAY, AND  
CENTRE OF MATHEMATICS FOR APPLICATIONS, UNIVERSITY OF OSLO, P.O. BOX 1053, BLINDERN, NO-0316 OSLO, NORWAY

*E-mail address:* holden@math.ntnu.no

*URL:* www.math.ntnu.no/~holden/

(Risebro)

CENTRE OF MATHEMATICS FOR APPLICATIONS, UNIVERSITY OF OSLO, P.O. BOX 1053, BLINDERN, NO-0316 OSLO, NORWAY

*E-mail address:* nilshr@math.uio.no

*URL:* folk.uio.no/nilshr/

(Sande)

DEPARTMENT OF MATHEMATICAL SCIENCES, NORWEGIAN UNIVERSITY OF SCIENCE AND TECHNOLOGY, NO-7491 TRONDHEIM, NORWAY

*E-mail address:* hildes@math.ntnu.no

*URL:* www.math.ntnu.no/~hildes/